A STEEP FAINT-END SLOPE OF THE UV LUMINOSITY FUNCTION AT $z \sim 2$–3: IMPLICATIONS FOR THE GLOBAL STELLAR MASS DENSITY AND STAR FORMATION IN LOW-MASS HALOS[*]

NAVEEN A. REDDY[1,3] AND CHARLES C. STEIDEL[2]

[1] National Optical Astronomy Observatory, 950 N. Cherry Ave., Tucson, AZ 85719, USA
[2] California Institute of Technology, MS 105–24, Pasadena, CA 91125, USA

ABSTRACT

We use the deep ground-based optical photometry of the Lyman Break Galaxy (LBG) Survey to derive robust measurements of the faint-end slope (α) of the UV luminosity function (LF) at redshifts $1.9 \leqslant z \leqslant 3.4$. Our sample includes > 2000 spectroscopic redshifts and ≈ 31000 LBGs in 31 spatially independent fields over a total area of 3261 arcmin^2. These data allow us to select galaxies to $0.07L^*$ and $0.10L^*$ at $z \sim 2$ and $z \sim 3$, respectively. A maximum-likelihood analysis indicates steep values of $\alpha(z = 2) = -1.73 \pm 0.07$ and $\alpha(z = 3) = -1.73 \pm 0.13$. This result is robust to luminosity-dependent systematics in the Lyα equivalent width and reddening distributions, and is similar to the steep values advocated at $z \gtrsim 4$, and implies that $\approx 93\%$ of the unobscured UV luminosity density at $z \sim 2$–3 arises from sub-L^* galaxies. With a realistic luminosity-dependent reddening distribution, faint to moderately luminous galaxies account for $\gtrsim 70\%$ and $\gtrsim 25\%$ of the bolometric luminosity density and present-day stellar mass density, respectively, when integrated over $1.9 \leqslant z < 3.4$. We find a factor of 8–9 increase in the star-formation rate density between $z \sim 6$ and $z \sim 2$, due to both a brightening of L^* and an increasing dust correction proceeding to lower redshifts. Combining the UV LF with stellar mass estimates suggests a relatively steep low-mass slope of the stellar mass function at high redshift. The previously observed discrepancy between the integral of the star-formation history and stellar mass density measurements at $z \sim 2$ may be reconciled by invoking a luminosity-dependent reddening correction to the star-formation history combined with an accounting for the stellar mass contributed by UV-faint galaxies. The steep and relatively constant faint-end slope of the UV LF at $z \gtrsim 2$ contrasts with the shallower slope inferred locally, suggesting that the evolution in the faint-end slope may be dictated simply by the availability of low-mass halos capable of supporting star formation at $z \lesssim 2$.

Key words: galaxies: evolution – galaxies: formation – galaxies: high-redshift – galaxies: luminosity function, mass function

Online-only material: color figures

1. INTRODUCTION

The last decade has seen significant advances in our understanding of the history of star formation and stellar mass assembly. Today, one can find several hundred determinations of the star-formation rate density (SFRD) estimated from observations at many wavelengths across a large range of lookback time. Taken together, these observations suggest a rapid increase in the SFRD from the epoch of reionization to $z \sim 1$–2, after which time the SFRD steadily decreased over the last ~ 10 billion years. This picture is generally understood in the context of hierarchical buildup at early times and gas exhaustion or heating at late times. While this characterization of the star-formation history is broadly accepted, there are several key details that are missing from this interpretation, including the potentially important contribution of UV-faint (sub-L^*) galaxies to the census of star formation and baryon budget. If rest-UV/optical light is a biased tracer of galaxy formation—particularly at high redshift where most of the baryons in galaxies are likely to reside in cold gas (Prochaska & Tumlinson 2008)—then faint galaxies may constitute an important population for studying the process of star formation and feedback. Furthermore, the number density of both bright and faint galaxies departs significantly from expectations based on the ΛCDM model, suggesting a regulation of star formation in both luminosity regimes. In this paper, we present an extension of our previous work on the UV luminosity function (LF) at $z \sim 2$–3 in order to provide robust constraints on the prevalence of UV-faint galaxies at epochs when galaxies were forming most of their stars.

The LF is a fundamental probe of galaxy formation and evolution, and can be used to address the relative importance of bright and faint galaxies to the energy budget at a given epoch. Furthermore, a comparison with the dark matter halo distribution informs us of the efficiency of star formation and effects of feedback at different mass scales (Rees & Ostriker 1977; Silk & Rees 1998; Dekel & Birnboim 2006). Therefore, constraining accurately the shape of the LF is a necessary step in acquiring a more complete census of galaxies and elucidating the relationship between the baryonic processes that govern galaxy evolution and the dark matter halos that host them.

The UV LF is relevant in several respects. Rest-frame UV emission is a direct tracer of massive star formation, modulo the effects of dust. Rest-frame UV observations of high redshift galaxies are generally not limited by spatial resolution and the deepest observations are up to a factor of ≈ 2000 times more sensitive than those in the infrared and longer wavelengths. The combination of resolution, sensitivity, and the accessibility of UV wavelengths over almost the entire age of the universe makes the UV LF a unique tool in assessing the star-formation history. The relative efficiency of UV-dropout selection has

enabled a number of investigations of the UV LF at high redshifts based on photometrically selected samples (Steidel et al. 1999; Adelberger & Steidel 2000; Yan & Windhorst 2004; Bunker et al. 2004; Dickinson et al. 2004; Bouwens et al. 2007; Sawicki & Thompson 2006; Reddy et al. 2008; Ouchi et al. 2004; Beckwith et al. 2006; Yoshida et al. 2006; Iwata et al. 2007).

Apart from the uncertainties that can be constrained from photometry alone, such as photometric errors and field-to-field variations, spectroscopy is a critical means of quantifying several important systematics that can affect the LF. These include contamination from low redshift objects and high redshift active galactic nuclei and quasi-stellar objects (AGNs/QSOs), attenuation of UV emission due to the opacity of the intergalactic medium (IGM), and perturbation of galaxy colors due to Lyα, reddening, and stellar population ages of galaxies. The relevance of these systematic effects is underscored by the fact that while there are numerous studies of the UV LF, the results have been inconsistent, both at low ($z \lesssim$ 3; e.g., Reddy et al. 2008; Le Fèvre et al. 2005) and at high ($z \gtrsim$ 4; e.g., Beckwith et al. 2006; Bouwens et al. 2007) redshifts.

Unfortunately, spectroscopic surveys have been limited to UV-bright ($\mathcal{R} \lesssim$ 25.5) galaxies at relatively low redshifts ($z \lesssim$ 4) and spectroscopic constraints on the number density of faint sources at $z \gtrsim$ 2 are still lacking. Deeper spectroscopy is expensive and will remain so until the next generation of large ($\gtrsim$ 10 m) ground-based telescopes come online. Given the present practical limitations and the complexity of systematics involved in computing LFs, it seems prudent to revisit and extend our initial estimate of the UV LF (Reddy et al. 2008, hereafter R08) by evaluating the impact of these systematics on the inferred number density of faint galaxies at $z \sim$ 2–3. We go beyond the initial analysis of R08 by quantifying several important effects relevant in the computation of star-formation rate (SFR) and stellar mass densities, including the effects of luminosity-dependent dust corrections and the integrated stellar mass of low-mass galaxies.

To this end, we combine what we know about the spectroscopic properties of Lyman Break Galaxies (LBGs) at $z \sim$ 2–3 with deep ground-based optical data in 31 spatially independent fields to determine the faint-end slope with greater precision. A brief description of the LBG survey, photometry, and follow-up spectroscopy is given in Section 2. Our method for computing the UV LF is presented in Section 3, and results are discussed in Section 4. Our results are compared with those in the literature and analyzed in the context of the early Hubble Deep Field (HDF) results, and we assess the impact of sample variance in Section 5. The evolution of the UV LF is quantified in Section 6. The contribution to the faint-end population from dusty, star-forming galaxies as well as quiescently evolving galaxies with large stellar masses is discussed in Section 7. Sections 8 and 9 present constraints on the SFRD and its evolution. We also reassess the stellar mass density at $z \sim$ 2 and compare it to inferences from integrating the star-formation history. Finally, the evolution of the faint-end slope of the UV LF is discussed briefly in Section 10. All magnitudes are expressed in AB units, unless stated otherwise. Unless indicated, a Kroupa (2001) IMF is assumed. A flat ΛCDM cosmology is assumed with $H_0 = 70$ km s^{-1} Mpc^{-1}, $\Omega_\Lambda = 0.7$, and $\Omega_m = 0.3$.

2. DATA: SAMPLE SELECTION AND SPECTROSCOPY

2.1. Fields and Photometry

The LBG survey is being conducted in fields chosen primarily for having relatively bright background QSOs with which to study the interface between the IGM and galaxies at $z \sim$ 2–3 (Adelberger et al. 2003, 2004, 2005b; Steidel et al. 2003, 2004). Additionally, the survey was extended to include fields that are the focus of multiwavelength campaigns, including the Groth–Westphal (Steidel et al. 2003; Groth et al. 1994) and GOODS-North fields (Dickinson et al. 2003; Giavalisco et al. 2004b). Presently, the survey includes 31 fields, 29 of which have been targeted spectroscopically (see R08 for further details). As emphasized throughout this paper, the large number of spatially independent fields provides a precise handle on the magnitude of sample variance, an effect that has limited the conclusions that could be drawn from previous determinations of the LF. For this analysis, we have included two additional fields beyond the 29 that were presented in R08, "Q1603" and "Q2240." Instruments used and dates of observation are presented in Steidel et al. (2003, 2004). For ease of reference, the fields are listed in Table 1; together they include an area of 3261 arcmin^2, or 0.91 square degrees.

Excepting Q1603, a modified version of FOCAS (Valdes 1982) was used to extract photometry from the optical ($U_n G \mathcal{R}$) images of the survey fields. Source Extractor (Bertin & Arnouts 1996) was used for photometry in Q1603. We took care to minimize systematics between the FOCAS and Source Extractor results for Q1603 from an examination of the color distribution of recovered LBG candidates. Object detection was done at $\mathcal{R}$ band, and $G - \mathcal{R}$ and $U_n - G$ colors were computed by applying the isophotal aperture from the $\mathcal{R}$-band image to the U_n and G images. Further details on the photometry are discussed in Steidel et al. (2003, 2004). The images have a 5 σ depth of 27.5–29.5 AB as measured through a $\sim$ 3$''$ diameter aperture.

2.2. Color Selection

We used the BX and LBG criteria which are based on the rest-frame UV colors expected of galaxies at redshifts 1.9 $\lesssim z \lesssim$ 2.7 and 2.7 $\lesssim z \lesssim$ 3.4, respectively (Steidel et al. 2004, 2003). For the spectroscopic follow-up, the sample of candidates was limited to $\mathcal{R} = 25.5$. However, because we are interested in using the entire photometric sample to constrain the LF at 1.9 $\lesssim z \lesssim$ 3.4, we did not impose this restriction. Rather, the detection significance and color distribution of candidates were examined to establish a faint limit. The limits applied to each field and numbers of candidates are listed in Table 1. Fields with the deepest imaging in the survey allow us to select candidates to $\mathcal{R} \sim 26.5$ with a detection completeness of $\approx 60\%$, based on the simulations described below. Our maximum-likelihood method for computing the LF allows us to extend the absolute magnitude limit ≈ 0.5 mag fainter given the broadness of the redshift distribution, $N(z)$, of the sample as constrained from an extensive spectroscopic follow-up. Even at these depths, galaxies are detected with typically $\gtrsim 5 \sigma$ significance in the $\mathcal{R}$ band. The photometric sample used here includes BX candidates in the original LBG survey fields where no spectroscopic follow-up of BX candidates was undertaken.

2.3. Spectroscopy

The spectroscopy of UV-selected candidates including LBGs and BXs is discussed in Steidel et al. (2003, 2004). To date, roughly 24% and 35% of BX and LBG candidates, respectively, with $\mathcal{R} < 25.5$ have been targeted spectroscopically. The resulting sample includes 2023 star-forming galaxies with 1.9 $\leqslant z_{\rm spec} <$ 3.4, the largest spectroscopic sample of star-forming galaxies at these redshifts. The spectroscopic statistics,

Table 1
Survey Fields

Field Name	α[a]	δ[b]	Field Size	$\mathcal{R}_{\mathrm{lim}}$	N_{BX}[c]	N_{LBG}[d]
	(J2000.0)	(J2000.0)	(arcmin^2)			
Q0000	00 03 25	−26 03 37	18.9	25.5	78	29
CDFa	00 53 23	12 33 46	78.4	26.0	490	192
CDFb	00 53 42	12 25 11	82.4	25.5	347	123
Q0100	01 03 11	13 16 18	42.9	26.5	579	230
Q0142	01 45 17	−09 45 09	40.1	26.0	379	158
Q0201	02 03 47	11 34 22	75.7	26.0	289	114
Q0256	02 59 05	00 11 07	72.2	25.5	325	105
Q0302	03 04 23	−00 14 32	244.9	25.5	2113	1025
Q0449	04 52 14	−16 40 12	32.1	26.5	287	138
B20902	09 05 31	34 08 02	41.8	25.5	229	72
Q0933	09 33 36	28 45 35	82.9	26.0	723	313
Q1009	10 11 54	29 41 34	38.3	26.5	512	305
Q1217	12 19 31	49 40 50	35.3	26.0	311	83
GOODS-N	12 36 51	62 13 14	155.3	26.0	496	154
Q1307	13 07 45	29 12 51	258.7	26.0	2011	718
Westphal	14 17 43	52 28 49	226.9	25.5	783	289
Q1422	14 24 37	22 53 50	113.0	26.0	1041	518
3C324	15 49 50	21 28 48	44.1	25.5	187	56
Q1549	15 51 52	19 11 03	37.3	26.0	329	153
Q1603	16 04 56	38 12 09	38.8	26.5	396	160
Q1623	16 25 45	26 47 23	290.0	26.0	1878	735
Q1700	17 01 01	64 11 58	235.3	26.0	2263	609
Q2206	22 08 53	−19 44 10	40.5	26.0	257	70
SSA22a	22 17 34	00 15 04	77.7	25.5	274	183
SSA22b	22 17 34	00 06 22	77.6	26.0	435	217
Q2233	22 36 09	13 56 22	85.6	26.0	420	173
DSF2237b	22 39 34	11 51 39	81.7	26.5	1004	474
Q2240	22 40 02	03 17 50	35.9	26.0	421	176
DSF2237a	22 40 08	11 52 41	83.4	26.5	553	183
Q2343	23 46 05	12 49 12	212.8	25.5	1209	436
Q2346	23 48 23	00 27 15	280.3	26.0	1547	472
TOTAL	...	...	3260.8	...	22166	8663

Notes.
[a] Right ascension in hours, minutes, and seconds.
[b] Declination in degrees, arcminutes, and arcseconds.
[c] Number of BX candidates to the limiting magnitude given in Column (5).
[d] Number of LBG candidates to the limiting magnitude given in Column (5).

including the number of spectroscopic redshifts, for each field of the LBG survey are given in R08.

The spectroscopic sample is used to estimate the overall contamination rate in the photometric sample. This contamination can arise from stars, low redshift galaxies and AGNs, as well as QSOs and AGNs at $1.9 \leqslant z < 3.4$. The contamination statistics and the extent to which they can be applied to determine the number of contaminants in the photometric sample are discussed in R08. Note that the contamination rate is a strong function of magnitude (being largest at bright magnitudes) and quantifying it is a crucial step in computing the bright end of the LF.

3. INCOMPLETENESS CORRECTIONS

3.1. Method

The approach that we adopted to correct the LBG sample for incompleteness and compute the UV LF is described in detail by R08. For convenience, here we summarize a few of the key features of our method. The primary goal is to construct a set of transformations that relate the observed properties of galaxies (e.g., observed luminosity, rest-frame UV slope, and redshift) to their true properties (e.g., intrinsic luminosity, reddening, and redshift). Using X-ray and mid-IR data for a sample of LBGs at

$z \sim 2$–3, Reddy et al. (2006b) demonstrate that the rest-frame UV slope can be used to measure the amount of dust reddening for typical LBGs, and we will assume this for the subsequent discussion.

We first used a Monte Carlo simulation to add galaxies of varying sizes and colors to our $U_nG\mathcal{R}$ images. The distribution of colors reflects that expected for star-forming galaxies at $z \sim 2$–3 with constant star formation for > 100 Myr and varying amounts of dust reddening. Specifically, we added objects with redshifts $1 < z < 4$ and reddening of $0.0 < E(B - V) < 0.6$. The simulated redshift is used to apply an IGM opacity to the colors using the Madau (1995) prescription. To make the simulation as realistic as possible, we forced the simulated galaxies to abide by a Schechter (1976) luminosity distribution and added just 100–200 of them at a time to the images. The latter restriction maintains the deblending statistics which in turn affect the photometric errors. Photometry was performed in the same manner as was used on the real data and the detection rate and recovered magnitudes and colors of the simulated galaxies were recorded. We repeated this procedure until $\approx 2 \times 10^5$ galaxies were added to the images in each field of the survey.

It is common to use such simulations to determine what fraction of galaxies with a given magnitude will be detected with colors that satisfy the LBG selection criteria. However, strictly speaking, the simulation will only tell us the probability that galaxies with a given *simulated* magnitude will be detected with a given *recovered* magnitude, and there may not be a monotonic correspondence between simulated and recovered magnitude. More generally, it is not necessarily true that the average simulated properties of galaxies are equivalent to their average observed properties. This is particularly true if photometric errors have significant biases and are comparable to the bin sizes used to compute the LF and the selection window spans a region of color space not much larger than the typical photometric errors. Other systematic effects, such as the Lyα equivalent width distribution ($W_{\mathrm{Ly}\alpha}$) of the population, may scatter galaxies in certain directions of color space. Also, some galaxies with simulated colors that do not initially satisfy the color criteria may have recovered colors that do: by definition, these galaxies' simulated properties will not, on average, reflect their observed properties. Because of these systematic effects, the number of galaxies that lie in a particular bin of observed properties will be some weighted combination of the number of galaxies in any number of bins of simulated properties.

Because of these systematic effects, we approach the problem of incompleteness by using the maximum likelihood method described in R08. Using this formalism, our goal is to maximize the likelihood of a given set of luminosity, reddening, and redshift distributions, denoted by $\mathcal{L}$, according to the following expression:

$$-\ln \mathcal{L} \propto \sum_{ijk} \bar{n}_{ijk} - \sum_{ijk} n_{ijk} \ln \bar{n}_{ijk}, \qquad (1)$$

where $\bar{n}_{ijk}$ is the expected number of galaxies in the ith bin of luminosity, jth bin of reddening, and kth bin of redshift that the values of the luminosity, reddening, and redshift distributions imply and n_{ijk} is the observed number of galaxies in that bin. The Monte Carlo simulations give the probability that a galaxy in the $i'j'k'$ bin of simulated properties will lie in the ijk bin of recovered properties. The set of probabilities, defined as the transitional probability function,

$$\xi \equiv \{p_{i',j',k' \to ijk}\}, \qquad (2)$$
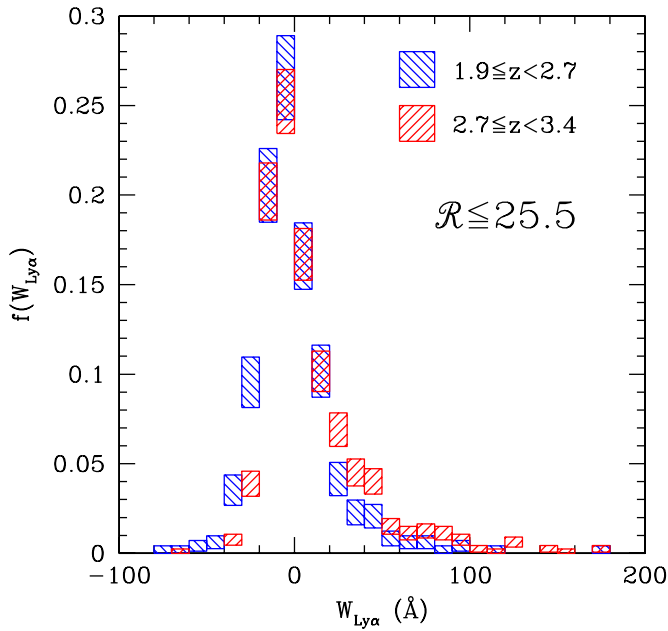
Figure 1. Intrinsic rest-frame Lyα equivalent width ($W_{\mathrm{Ly}\alpha}$) distribution for $\mathcal{R} \leqslant 25.5$ star-forming galaxies at $1.9 \leqslant z < 2.7$ and $2.7 \leqslant z < 3.4$, from R08. Lyα in emission is represented as $W_{\mathrm{Ly}\alpha} > 0$. Error bars are determined from simulations and reflect the variance in the distributions allowed by the errors in the UV LF and reddening distribution (see R08 for discussion).

(A color version of this figure is available in the online journal.)

is used to compute $\bar{n}_{ijk}$. The basic procedure is then to vary the input distributions of luminosity, reddening, and redshift until the differences between the expected and observed numbers of galaxies in each ijk bin are minimized.

3.2. Lyα Equivalent Width ($W_{\mathrm{Ly}\alpha}$) Distribution

An important systematic effect to consider is the scattering of colors due to the presence of Lyα emission and absorption: the Lyα line falls within the U_n and G bands at redshifts that are targeted with the BX and LBG criteria, the same bands that are used to select the galaxies. Rather than adding the $W_{\mathrm{Ly}\alpha}$ distribution as another free parameter in the maximum-likelihood analysis—thus complicating our ability to determine the LF—we performed simulations where we made various assumptions regarding the intrinsic $W_{\mathrm{Ly}\alpha}$ distribution at $z \sim 2$–3 and observed the effects on the best-fit LF (R08). We did this by adding a random $W_{\mathrm{Ly}\alpha}$ drawn from a distribution of $W_{\mathrm{Ly}\alpha}$ to each galaxy, and then recomputing the colors of each galaxy. Effectively, the addition of Lyα will perturb the colors and thus modulate the transitional probability function, ξ. R08 showed that the BX and LBG color criteria did little to alter the intrinsic $W_{\mathrm{Ly}\alpha}$ distribution at $z \sim 2$ and $z \sim 3$. Therefore, we assume the $W_{\mathrm{Ly}\alpha}$ distribution observed for BXs and LBGs (Figure 1). Here, we not only repeat the simulations of R08, but also allow for changes in the shape of the $W_{\mathrm{Ly}\alpha}$ distribution proceeding from UV-bright to UV-faint galaxies (see Appendices).

4. RESULTS: THE UV LF AT $1.9 \leqslant z < 3.4$

4.1. Computation of the LF and Errors

The value of the luminosity distribution that maximizes the likelihood of observing our data (Equation (1)) is computed using the method discussed in the previous section. Initially, we assumed that the intrinsic distributions of (1) rest-frame

UV slopes, (2) redshifts, and (3) $W_{\mathrm{Ly}\alpha}$ remain constant as a function of apparent magnitude. In R08, we justified these assumptions when computing the LF to our spectroscopic limit of $\mathcal{R} = 25.5$. However, it is not unreasonable to suspect that, for example, the reddening and $W_{\mathrm{Ly}\alpha}$ distributions of galaxies fainter than our spectroscopic limit may be different than those for galaxies where we are able to directly measure the distributions with spectroscopy (spectroscopic distributions). Such differences will change ξ and thus affect our incompleteness corrections. First, we made the simplified assumptions that all of these distributions remain unchanged as a function of apparent magnitude. LFs derived in this case are referred to as the "fiducial" LFs. In the Appendices, we discuss how the LF would change if we adopt more realistic assumptions for the properties of UV-faint galaxies. In our analysis, the effect of increasing photometric error for fainter galaxies is already incorporated in the calculation of ξ.

LFs were computed separately for star-forming galaxies in the redshift ranges $1.9 \leqslant z < 2.7$ and $2.7 \leqslant z < 3.4$ using the photometric BX and LBG samples, respectively. For the lower redshift range, the LF is computed in terms of a (composite) absolute magnitude that is the average of the G and $\mathcal{R}$-band fluxes. For the higher redshift range, the LF is computed using the $\mathcal{R}$-band magnitude. This method provides the closest match between rest-frame wavelengths, roughly 1700 Å.

The total error in the LF is computed using the following method. The observed number counts of galaxies in each field were adjusted randomly in accordance with a Poisson distribution and the maximum-likelihood LF was computed for each field. This procedure was repeated many times for all the fields. The dispersion in the LF values for each bin in absolute magnitude is taken as the total error which, as a consequence of the way in which it is computed, includes both Poisson and field-to-field variations.

4.2. Summary of Systematic Effects and Final Results

The details of the systematic tests performed to judge the effects of luminosity-dependent $W_{\mathrm{Ly}\alpha}$ and reddening distributions on the LF are presented in the Appendices. To summarize, we analyzed the influence of galaxies with (1) strong Lyα emission and (2) zero or declining reddening with apparent UV magnitude. Employing current estimates of the mean stellar population, reddening, and number density of galaxies with strong Lyα emission as a function of UV luminosity at high redshifts, we find that the inferred number density of galaxies on the faint end of the UV LF increases by $\lesssim 3\%$ at $1.9 \leqslant z < 2.7$ and decreases by $\lesssim 4\%$ at $2.7 \leqslant z < 3.4$. Because these changes are not negligible compared to the Poisson and field-to-field errors on the faint-end number densities, they should be included in any proper assessment of the LF. Nonetheless, these changes in number density can be accommodated by Schechter parameterizations that vary within the uncertainties of the individual parameters, α, M^*, and ϕ^*.

We have also examined how changes in the mean reddening of galaxies as a function of UV luminosity affects our measurement of the UV LF. We considered two scenarios, one in which the extinction drops to zero for galaxies fainter than $\mathcal{R} = 25.5$ and one in which the extinction decreases monotonically with UV luminosity, and approaches zero in the faintest luminosity bin considered here. The latter scenario is more realistic than the former, and is parameterized as a linear relation between $E(B - V)$ and magnitude (see the Appendices; we refer to this latter scenario as the "luminosity-dependent reddening model").
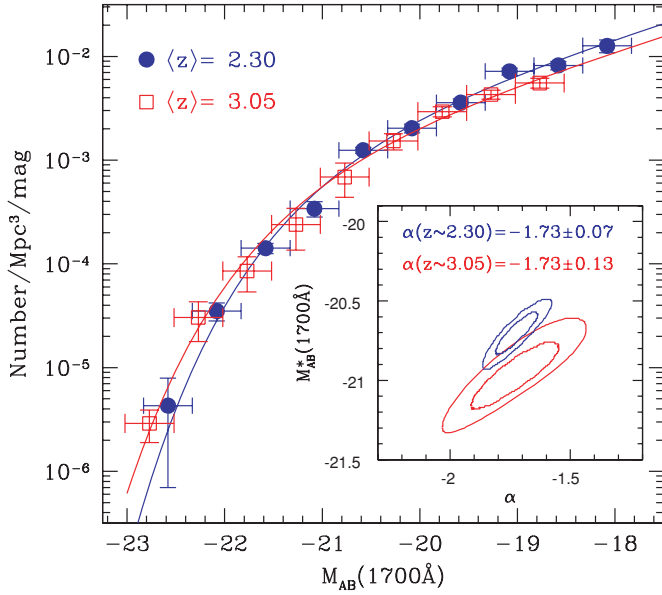
Figure 2. Rest-frame UV LFs of star-forming galaxies at $1.9 \leqslant z < 2.7$ (circles) and $2.7 \leqslant z < 3.4$ (squares), along with the best-fit Schechter (1976) functions. The 68% and 95% likelihood contours between M^* and α for our final determinations of the LFs are shown in the inset panel.

(A color version of this figure is available in the online journal.)

Table 2
Rest-Frame UV LFs of $1.9 \lesssim z \lesssim 3.4$ Galaxies

Redshift Range	$M_{AB}(1700 \text{ Å})$	ϕ $(\times 10^{-3} \, h_{0.7}^3 \, \text{Mpc}^{-3} \, \text{mag}^{-1})$
$1.9 \leqslant z < 2.7$	-22.83 to -22.33	0.004 ± 0.003
	-22.33 to -21.83	0.035 ± 0.007
	-21.83 to -21.33	0.142 ± 0.016
	-21.33 to -20.83	0.341 ± 0.058
	-20.83 to -20.33	1.246 ± 0.083
	-20.33 to -19.83	2.030 ± 0.196
	-19.83 to -19.33	3.583 ± 0.319
	-19.33 to -18.83	7.171 ± 0.552
	-18.83 to -18.33	8.188 ± 0.777
	-18.33 to -17.83	12.62 ± 1.778
$2.7 \leqslant z < 3.4$	-23.02 to -22.52	0.003 ± 0.001
	-22.52 to -22.02	0.030 ± 0.013
	-22.02 to -21.52	0.085 ± 0.032
	-21.52 to -21.02	0.240 ± 0.104
	-21.02 to -20.52	0.686 ± 0.249
	-20.52 to -20.02	1.530 ± 0.273
	-20.02 to -19.52	2.934 ± 0.333
	-19.52 to -19.02	4.296 ± 0.432
	-19.02 to -18.52	5.536 ± 0.601

In this case, we find appreciable increases of $\approx$ 10% in the inferred number density between $1.9 \leqslant z < 2.7$. In the higher redshift range $2.7 \leqslant z < 3.4$, there is little change in the inferred number densities. Our final determinations of the LF and the corresponding Schechter fits are shown by the data points and solid lines, respectively, in Figure 2, with the values and Schechter parameterization listed in Tables 2 and 3.

Our determinations of the bright end of the UV LFs to $M(1700 \text{ Å}) = -18.83$ and -19.52 at $z \sim 2$ and $z \sim 3$, respectively, incorporate data over 3261 arcmin^2 in 31 independent fields. Data from 22 fields and 2239 arcmin^2 are used to constrain the LFs at $-18.83 \leqslant M(1700 \text{ Å}) < -18.33$ and $-19.52 \leqslant M(1700 \text{ Å}) < -19.02$ at $z \sim 2$ and $z \sim 3$,
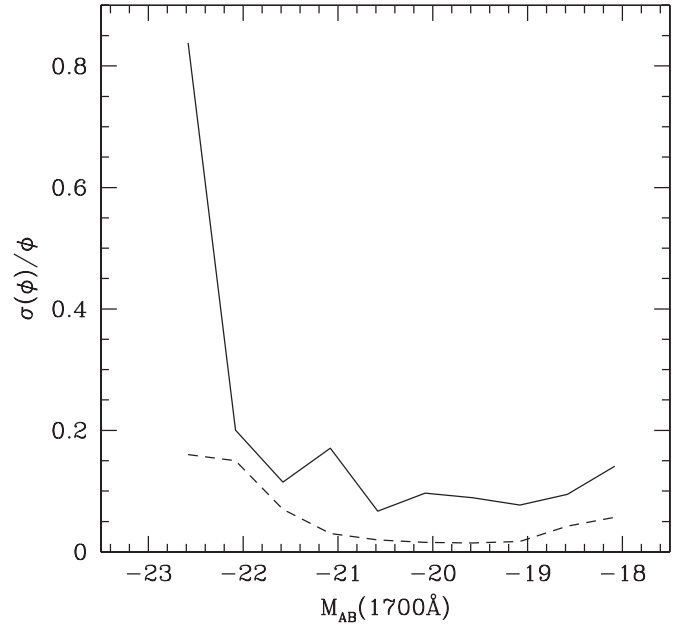
Figure 3. Poisson (dashed line) and total (solid line) error in the UV LF at $z \sim 2$. The Poisson error increases to fainter magnitudes given the smaller survey area used to constrain the faint end. At all magnitudes, however, the error in the LF is dominated by field-to-field variations. Similar results are obtained for the $z \sim 3$ UV LF.

Table 3
Best-Fit Schechter Parameters for UV LFs of $1.9 \lesssim z \lesssim 3.4$ Galaxies

Redshift Range	α	$M_{AB}^*(1700 \text{ Å})$	$\phi^* (\times 10^{-3} \text{ Mpc}^{-3})$
$1.9 \leqslant z < 2.7$	-1.73 ± 0.07	-20.70 ± 0.11	2.75 ± 0.54
$2.7 \leqslant z < 3.4$	-1.73 ± 0.13	-20.97 ± 0.14	1.71 ± 0.53

respectively. Finally, data from six spatially independent fields and 317 arcmin^2 are used to constrain the LF in the faintest magnitude bin to $M(1700 \text{ Å}) = -17.83$ and -18.52 at $z \sim 2$ and $z \sim 3$, respectively. To ensure that spatial variance in these six deep fields is not driving the observed faint-end slope, we recalculated α by fitting Schechter functions to the LFs excluding the faintest bin. Allowing ϕ^* and M^* to vary, we calculate $\alpha = -1.75 \pm 0.09$ and -1.94 ± 0.18 at $z \sim 2$ and $z \sim 3$, respectively, still significantly steeper than the shallower $\alpha > -1.6$ found in previous studies. The similarity in α obtained with or without data from the faintest bin is not surprising given that the uncertainty in the LF includes the sample variance from the six fields used to constrain the number density in this bin.

The degeneracy between the faint-end slope (α) and characteristic magnitude (M^*)—illustrated by the likelihood contours in Figure 2 (inset)—is reduced significantly compared to that computed in R08. Our analysis extends to luminosities that are four times fainter than the limit dictated by efficient spectroscopy, and $\approx$ 14 and 10 times fainter, respectively, than the characteristic luminosity L^* at $z \sim 2$ and 3. Our sample is large enough so that the error in the LF at all magnitudes is dominated by field-to-field variations (Figure 3). Within the total errors, the UV LFs at $z \sim 2$ and $z \sim 3$ are virtually indistinguishable, indicating little change between the two in the number density of both UV-bright and UV-faint galaxies.

5. DISCUSSION: LARGE-SCALE CONTEXT

In the following sections, we discuss our results in the context of previous determinations of the UV LF (Section 5.1) and its
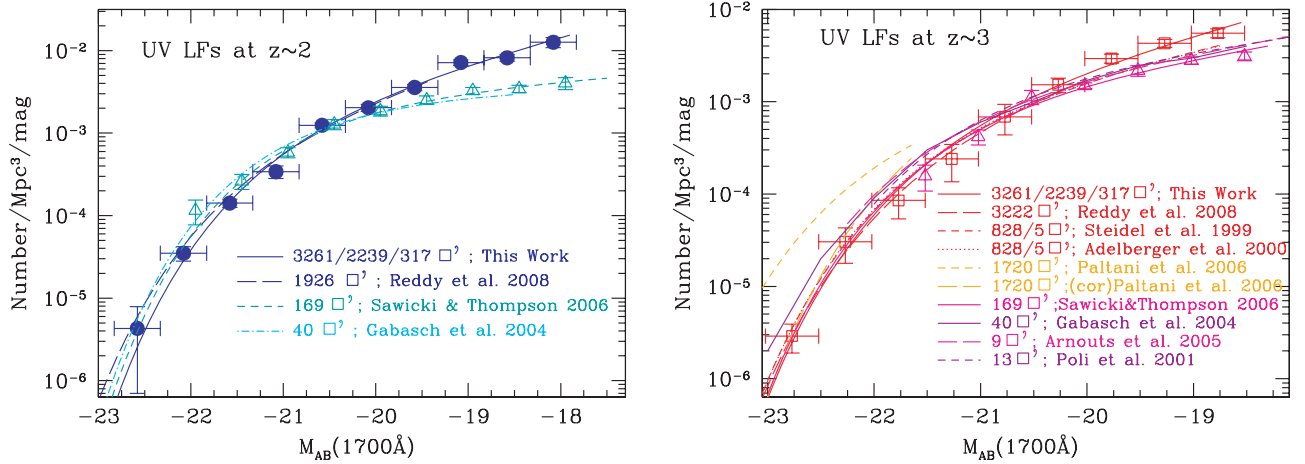
Figure 4. Comparison of UV LFs at $z \sim 2$ (left) and $z \sim 3$ (right). For clarity, data points are excluded on all but our current determinations and those of Sawicki & Thompson (2006), but the errors are typically smaller than the observed differences discussed in the text. Also shown are the survey areas over which the LF is derived, with some surveys using a combination of wider shallower data to anchor the bright end of the LF and deeper data in smaller areas to constrain the faint-end slope. Included are data from Reddy et al. (2008); Sawicki & Thompson (2006); Paltani et al. (2007); Arnouts et al. (2005); Gabasch et al. (2004); Poli et al. (2001); Adelberger & Steidel (2000); Steidel et al. (1999).

(A color version of this figure is available in the online journal.)

evolution with redshift (Section 6). To gain further insight into the nature of sub-L^* galaxies, we assess the contribution to the faint-end population from dusty, star-forming galaxies, and those with large stellar masses (Section 7). In Section 8, we discuss the implications of a luminosity-dependent reddening distribution and the average corrections required to recover the bolometric SFRD. These findings are then discussed in the context of the star-formation history and the buildup of stellar mass in Section 9. Finally, we discuss briefly the evolution of the faint-end slope in Section 10.

5.1. Comparisons at $z \sim 2$–3

In this section, we place our results in the context of previous determinations of the UV LFs, starting with those around $z \sim 2$. Figure 4 summarizes the results of several previous studies including those of Gabasch et al. (2004), Sawicki & Thompson (2006), and R08, along with our current determination, at $z \sim 2$. The redshift intervals over which the LF is computed are similar between these studies, but we note the almost two orders of magnitude difference in the areas probed, from ≈ 40 arcmin^2 at the low end to 3261 arcmin^2 in the current determination. There are significant differences between the LFs at faint magnitudes ($M(1700$ Å$) \gtrsim -20$). In general, it is possible that the determinations of the smaller surveys (e.g., from the FORS-Deep Field; Gabasch et al. 2004) could be mimicked by an overall under-density in the small area probed combined with an overestimation of the bright end due to contamination from low-redshift interlopers. Gabasch et al. (2004) do not specify the contamination fractions for their higher redshift samples at $z \gtrsim 2$, so a fair comparison with our findings at the bright end is not possible. We also note that Gabasch et al. (2004) relied on photometric redshifts which could not be well calibrated due to the lack of spectroscopically confirmed galaxies at $z \sim 2$ examined in their study (see their Figure 2). R08 showed that biases in photometric redshifts can easily boost the bright end of the LF with respect to the faint end, and the overall shape of their LF may be a result of this effect.

Perhaps a fairer comparison can be made with Sawicki & Thompson (2006) since they use exactly the same filter set to select BX candidates at $z \sim 2.3$ in the Keck Deep Fields

(KDFs). For their fiducial model, they assumed no perturbation of colors due to Lyα and a constant $E(B - V) = 0.15$ with no dispersion, and they compute the LF using the standard $V_{\rm eff}$ method. Their LF suggests a much shallower slope of $\alpha \sim -1.2$ compared to our result (Figure 4). However, Sawicki & Thompson (2006) point out that their LF derived at $z \sim 2$ is sensitive to the assumed $E(B - V)$, and that bluer values of $E(B - V)$ will tend to yield larger inferred number densities (see their Figure 7). This observation is consistent with our finding and, in particular, if the $E(B - V)$ distribution becomes significantly bluer proceeding to fainter galaxies, this effect would manifest itself as a steepening of the faint-end slope (Appendices). However, this systematic effect alone cannot account for all of the difference between our result and that of Sawicki & Thompson (2006), since even in the fiducial case of a luminosity-invariant $E(B - V)$ distribution (but not constant valued) we find a steep $\alpha = -1.67 \pm 0.06$ (Appendices). In any case, regardless of how the mean $E(B - V)$ varies with magnitude, the distribution itself is not a delta function, of course, and has intrinsic dispersion; those galaxies at the blue end of the distribution (i.e., less reddening) will tend to escape the selection criteria more frequently than galaxies with redder $E(B - V)$. Hence, a bluer mean $E(B - V)$, the intrinsic scatter in $E(B - V)$ for UV-faint galaxies, and a general perturbation of colors due to Lyα will all result in larger corrected number densities at the faint end.

Focusing on the higher redshift range, we find again reasonable agreement among the various determinations of the bright end of the UV LF at $z \sim 3$.[4] The only significantly discrepant points are from the VVDS that imply significant numbers of UV-bright galaxies (Paltani et al. 2007). However, applying the correct contamination fractions (based on spectroscopy) to their points brings them in accordance with the other determinations (R08). As at lower redshifts, we find a substantially steeper faint-end slope at $z \sim 3$ than suggested by previous results. Most determinations have found $\alpha > -1.6$, shallower than the canonical $\alpha = -1.6$ from Steidel et al. (1999), although most of

---

[4] Sawicki & Thompson (2006) use the results from Steidel et al. (1999) to constrain the bright end of the UV LF at $z \sim 3$.

these studies (including Steidel et al. 1999) constrained α using deep data from only one or two small deep fields (e.g., Hubble Deep Field, FORS Deep Field) where large-scale structure may be an issue. Sawicki & Thompson (2006) find $\alpha = -1.43^{+0.17}_{-0.09}$ based on the KDF data over an area of 169 arcmin^2.

5.2. Differences in LF Computation

What could be the reason for the disparity in the faint-end number densities between our study and previous determinations? Without a more detailed comparative analysis incorporating the data used in these other studies, it is difficult to pinpoint a single cause for the discrepancy. There are, however, a number of differences between our analysis and others that may lead to the observed variance in α. Our analysis (1) uses over 2000 spectroscopic redshifts to evaluate and correct for contamination as a function of luminosity; (2) models the systematic effects of a luminosity dependence in the intrinsic Lyα equivalent width and reddening distribution of galaxies, likely to be the two dominant sources of systematic error in the LF; (3) employs a maximum-likelihood method that is more robust than the $V_{\rm eff}$ method against biases in photometry and other nonuniform sources of scatter; and (4) takes advantage of data in 31 spatially uncorrelated fields over a total area of close to a square degree. Even at the faint end, our determinations are based on six independent fields with a total area of 317 arcmin^2, a roughly 88% larger area than used in the previous faint-end determination at $z \sim 2$–3 (but see the next section). For all of these reasons, we believe our LFs to be the most robust determinations to date.

The differences in faint-end slope derived between studies with similar depth is not particularly significant within the marginalized errors on α. For example, the $\alpha = -1.43^{+0.17}_{-0.09}$ of Sawicki & Thompson (2006) is still consistent within the 1 σ (marginalized) error of our determination of $\alpha = -1.73 \pm 0.13$ at $z \sim 3$. Yet the difference in the actual number density of faint galaxies is significant at the 2–3 σ level. This emphasizes why comparisons between α derived in different studies should perhaps not be taken too seriously without placing them in the context of the errors on the actual number density of UV-faint galaxies.

5.3. Cosmic Variance

In spite of the care used in the present sample, even 317 arcmin^2 is a relatively small area over which to constrain α. As noted above, the uncertainties in the LF are dominated by field-to-field variance at all magnitudes. We can assess how the empirically constrained errors on the UV LF compare to expectations based on the correlation function. Following the procedure outlined by Trenti & Stiavelli (2008), we can estimate the combined uncertainty due to cosmic variance and Poisson statistics by integrating the two-point correlation function for dark matter halos with some average galaxy bias. The basic premise is that the spatial correlation function of halos gives information on the variance in the spatial distribution of galaxies along different lines of sight given various assumptions for the cosmology and halo filling factor. For this calculation, we assumed a number density of objects as implied by the maximum-likelihood LF at $z \sim 2$ and a sample "completeness" fraction of 0.47. This number is the ratio of star-forming galaxies that satisfy the color selection criteria to the total number of star-forming galaxies as determined from the LF (see R08 for a discussion of this fraction). The cosmology is set as follows: $\Omega_\lambda = 0.74$, $\Omega_m = 0.26$, $H_0 = 70$ km s^{-1} Mpc^{-1}, a spectral

index $n_{\rm s} = 1$, and $\sigma_8 = 0.9$ (Spergel et al. 2007). We must also make some assumption for the halo filling factor. Star-forming galaxies are scattered out of the LBG selection window due to primarily random processes such as photometric scatter (Reddy et al. 2005), and must therefore cluster in the same way as galaxies that do satisfy the LBG criteria (Conroy et al. 2008). Furthermore, the comoving number density of LBGs is similar to the number density of halos that have similar clustering strength, suggesting a halo filling factor of ≈ 1 (Conroy et al. 2008). Assuming this remains valid for UV-faint galaxies, we find a fractional error in number counts of $\approx 9\%$ over a survey area of 317 arcmin^2. In general, we would expect this calculation to yield a lower limit to the uncertainty since other effects (e.g., uncertainties in zeropoints and systematics in the color distributions from field to field) contribute to the error in the LF, and indeed our empirically derived error in the faintest bin of the $z \sim 2$ UV LF is $\approx 50\%$ larger than the value obtained from the two-point correlation function. For comparison, this calculation implies that the field-to-field variance is $\approx 17\%$ lower than what we would have obtained over the area probed by the KDFs of 169 arcmin^2 (Sawicki & Thompson 2006). This difference is not large enough to explain the apparent discrepancy at the faint end, and some of the systematics discussed above are also likely to play a role. Deep UV imaging over areas of close to a square degree (similar to that used to estimate the bright end of the LF) will be required to constrain the fractional error in number counts to $\lesssim 5\%$.

5.4. Hubble Deep Field (HDF)

A comparison between the present work and those of the early HDF-based studies of the UV LF is useful, particularly in light of the often-used argument that the HDF presents a biased view of the universe, and one that is invoked to explain the divergent results on the UV LF at $z \sim 3$ (Steidel et al. 1999; Dickinson et al. 2003; Giavalisco et al. 2004a; Gabasch et al. 2004; Sawicki & Thompson 2006). The bright end of the LFs computed here and by Steidel et al. (1999) are in excellent agreement. Within the 1σ marginalized errors, the faint-end slope derived at $z \sim 3$ agrees with the slope found by Steidel et al. (1999) and Adelberger & Steidel (2000), and there is essentially no significant difference in ϕ^* and M^*. However, given the widespread use of the Steidel et al. (1999) results, it is important to note that their determination of α—constrained from a U-dropout sample in the HDF—does not take into account incompleteness from photometric scatter. As discussed in Section 3, the effect of such scatter is to make the incompleteness corrections larger at the faint end, thus steepening the faint-end slope. In summary, contrary to the suggestion that the HDF contained an over-density of faint galaxies relative to bright ones when compared with other fields, our results imply that the HDF is reasonably representative of the $z \sim 2$–3 universe.

6. DISCUSSION: EVOLUTION OF THE UV LF

Figure 5 summarizes our UV LFs at $z \sim 2$–3 along with higher redshift determinations. For clarity and consistency, we included the findings from Bouwens et al. (2007) only since those authors use a maximum-likelihood method for determining the LF that is similar to the method we use. These authors provide a detailed comparison of UV LFs at $z \gtrsim 4$ from different studies.
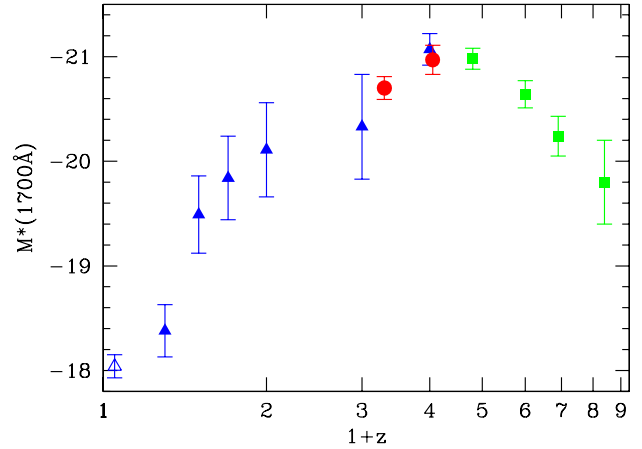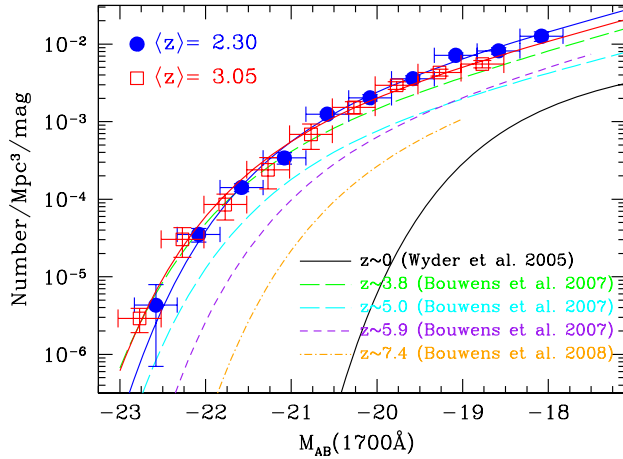
Figure 5. Left: evolution of the UV LFs from $z \sim 7$ to $z \sim 2$. For clarity and consistency, we show only LFs at $z \gtrsim 4$ from Bouwens et al. (2007, 2008) since they are calculated using a maximum-likelihood technique similar to the one used here. For comparison, the local UV LF from Wyder et al. (2005) is also shown. Right: evolution of the characteristic UV luminosity or magnitude, M^*, with redshift. Points are from Wyder et al. (2005) at $z \sim 0$ (open triangle), Arnouts et al. (2005) at $0 \lesssim z \lesssim 3.0$ (filled triangles), Bouwens et al. (2008) at $z \gtrsim 4$ (squares), and our determinations at $z \sim 2$–3 (circles).
(A color version of this figure is available in the online journal.)

6.1. Evolution in M^*

Despite the large number of investigations at $z \gtrsim 4$, there is still a fair amount of uncertainty regarding the parameterization of the evolution in the UV LF. Some have claimed that the evolution occurs primarily in L^* (Bouwens et al. 2007), while others find an evolution in ϕ^* (Beckwith et al. 2006) or the faint-end slope α (Iwata et al. 2007). Some have also suggested an evolution in both L^* and ϕ^* (e.g., Dickinson et al. 2004; Giavalisco et al. 2004a) such that the total luminosity density could remain constant from $z \sim 3$–6. Of course, the reach of some of these conclusions is limited by the depth of data used to derive the LF. Because the LFs at $z \gtrsim 2$ shown in Figure 5 are derived using data of comparable depth and analyzed in a similar manner—although we note that our LFs at $z \sim 2$–3 are anchored by spectroscopy and photometry in an area roughly an order of magnitude larger than used at $z \gtrsim 4$—hereafter we will assume that the evolution of the LF at $z \gtrsim 4$ can be accommodated by a change in L^* as advocated by Bouwens et al. (2007). Given the observed fading of galaxies at $z \lesssim 2$ (e.g., Dickinson et al. 2003; Madau et al. 1996; Lilly et al. 1995, 1996; Steidel et al. 1999), it is useful to examine our results in the context of this evolution in L^* (Figure 5). In particular, we find that L^* is brightest at $z \sim 2$–3, with this average unobscured UV luminosity decreasing at $z \gtrsim 4$ (earlier cosmic time) and decreasing by a factor of ≈ 16 between $z \sim 2$ and the present day. Quantitatively, Bouwens et al. (2008) found a linear parameterization between M^* and z at $z \gtrsim 4$ that appears to follow that generally expected for the growth of the halo mass function—assuming an evolution in the mass-to-light ratio for halos of $\sim (1+z)^{-1}$—given standard assumptions for the matter power spectrum, indicating that hierarchical assembly of halos may be dominating the evolution in M^*, or equivalently L^*. In the context of this study, the linear parameterization can be ruled out at the $8\,\sigma$ level at $z = 2.3$ (in the sense that it would predict a significantly larger L^* at $z = 2.3$ than is observed), indicating that by these redshifts, some other effect(s) modulate L^* away from the value expected from pure hierarchical assembly.

These observations are illustrated more clearly by examining dN/dz as a function of redshift (Figure 6), which is extrapolated based upon linearly fitting the relationship between L^* and z and ϕ^* and z, and assuming a fixed $\alpha = -1.73$ as indicated by

the Schechter fits (Table 3). Integrating the number counts to a *fixed* luminosity shows that bright galaxies with $L > 0.1L^*_{z=3}$ increase in number density by an order of magnitude with cosmic time from $z \sim 7$ to $z \sim 2$. Alternatively, the number counts are flatter at $z \gtrsim 4$ when integrating to $0.1L^*(z)$ (i.e., L^* appropriate at the redshift z where dN/dz is calculated) suggesting that ϕ^* is relatively constant at these redshifts (e.g., Bouwens et al. 2007). There may be a slight increase in ϕ^* between $z \sim 2$–3, though the magnitude of the errors on ϕ^* are large enough that we cannot rule out nonevolution in the number density.

Also shown is dL/dz, both above and below a fixed luminosity, in this case $0.1L^*_{z=3}$, along with the total luminosity density. The evolution implied by our LFs suggests that the approximately order of magnitude increase in luminosity density between $z \sim 7$ and $z \sim 4$ is followed by a flattening between $z \sim 2$–3. This result itself is hardly surprising (see Giavalisco et al. 2004a; R08), but its significance is constrained robustly given that our LFs are determined over two orders of magnitude in luminosity. We will return to a discussion of these findings in the context of the cosmic star-formation history (Section 8).

6.2. Evolution in α

Perhaps the most striking result of our analysis—and one that is possible to address with confidence given the depth of data considered here—is a very steep faint-end slope of $\alpha \sim -1.73$ at $z \sim 2$–3 that is robust to the luminosity-dependent systematics discussed in Appendices. The α we derive at $z = 2.30$ is virtually identical to that derived at $z = 3.05$, and is remarkably similar to the steep faint-end slopes favored at $z \gtrsim 4$ (Figure 7). Given the rapid evolution in L^* and the luminosity density at $z \gtrsim 2$, the invariance of α over the same ~ 3 Gyr time span and the shallow α found locally (Wyder et al. 2005; Budavári et al. 2005) pose interesting constraints on models of galaxy formation. We revisit this issue in Section 10.

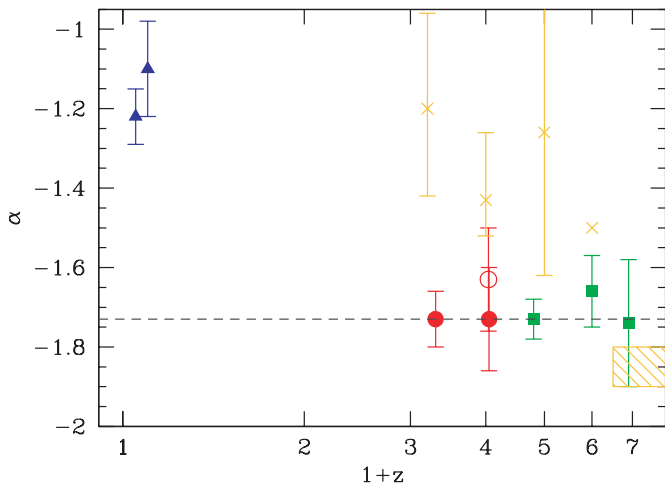## 7. DISCUSSION: NATURE OF GALAXIES ON THE FAINT END OF THE UV LF

Before proceeding to discuss the implications of our results, it is useful to assess the contribution of galaxies selected with different methods to the UV LF. R08 demonstrate that the BX
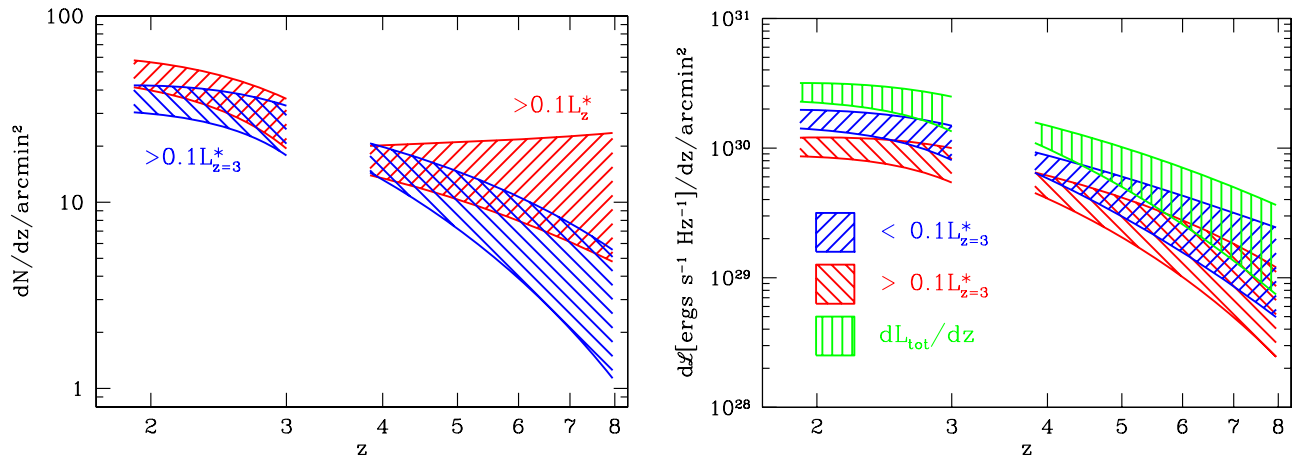
Figure 6. Left: dN/dz as a function of redshift, assuming our determinations of the UV LF at $z \sim 2$–3 and those of (Bouwens et al. 2007) at $z \gtrsim 4$, integrated to $0.1L^*_{z=3}$ (blue) and $0.1L^*_z$ (red). The shaded regions indicate approximately the uncertainty based on the errors in the Schechter parameters. Right: total dL/dz as a function of redshift (green) and dL/dz brighter and fainter than $0.1L^*_{z=3}$ (red and blue, respectively).

(A color version of this figure is available in the online journal.)

7.1. Bolometrically Luminous Galaxies

Deep mid-to-far-IR surveys have uncovered a sizable population of dusty and infrared luminous galaxies at $z \sim 2$–3 (e.g., Yan et al. 2007; Caputi et al. 2007; Papovich et al. 2007; Reddy et al. 2005; Chapman et al. 2005; van Dokkum et al. 2004; Smail et al. 1997; Barger et al. 1998). The first such galaxies were discovered via their submillimeter emission (Smail et al. 1997; Barger et al. 1998; Hughes et al. 1998), and are now commonly referred to as submillimeter galaxies (SMGs). Chapman et al. (2005) estimated that $\approx 65\%$ of such spectroscopically confirmed bright SMGs (e.g., with $S_{850\,\mu m} \gtrsim 5$ mJy) at $z \sim 2$–3 have rest-frame UV colors similar to those of BXs and LBGs, yet are on average a factor of ≈ 10 times more luminous. There is some uncertainty in the luminosities related both to the conversion between mid and IR luminosities to total bolometric luminosities and the fraction of the luminosity that arises from an AGN (Alexander et al. 2005). Taking the far-IR estimates of the SFRs of SMGs at face value then suggests that SMGs are examples of galaxies whose UV slopes typically underpredict their total attenuation and hence total bolometric luminosities (Reddy et al. 2006b).

Measuring the frequency of such dusty galaxies among UV-faint sources requires that we estimate the former's space density. Coppin et al. (2006) determine a surface density of SMGs with $S_{850\,\mu m} > 5$ mJy of 0.139 arcmin^{-2}. The spectroscopic study of Chapman et al. (2005) found that 50% of bright SMGs lie at redshifts $1.9 \leqslant z < 2.7$, implying a space density at these redshifts of 2.63×10^{-5} Mpc^{-3}. These authors also found 30–50% of them have $25.5 < \mathcal{R} < 28.0$, corresponding to $L_{UV} \lesssim 0.34L^*$ at the mean redshift of the BX sample ($z = 2.30$). According to our UV LF, the total number density of galaxies over this same apparent magnitude range is 3.28×10^{-2} Mpc^{-3}, implying that UV-faint SMGs with $\mathcal{R} > 25.5$ constitute 0.02–0.04% of sources on the faint end. Even in the most conservative case where we assume that all SMGs with $S_{850\,\mu m} > 5$ mJy lie at $1.9 \leqslant z < 2.7$ and all have $\mathcal{R} > 25.5$, we find a fractional contribution of only 0.16%. The results of Chapman et al. (2005) indicate that this SMG fraction would be even lower among $z > 2.7$ galaxies, although we note that their adoption of a radio-preselection may have biased the distribution of their sources to lower redshifts. We make note of the fact that the exact contribution will depend on the limit

Figure 7. Faint-end slope α as a function of redshift. At $z \gtrsim 2$, we include our results (filled circles), that of Steidel et al. (1999) (open circle), and those of Bouwens et al. (2007) (squares). At lower redshifts, we included only points in the Ryan et al. (2007) compilation that were derived from the rest-UV LF and that relied on data extending at least two magnitudes fainter than M^*, including results from Budavári et al. (2005) and Wyder et al. (2005) (triangles). Also shown are points from Sawicki & Thompson (2006), Iwata et al. (2003) (errors in α are not provided by these authors; crosses), and Yan & Windhorst (2004) (range of likely α indicated by the hashed box). The dashed line marks the mean value of α found at $z \gtrsim 2$ from our study and that of Bouwens et al. (2007) ($\langle \alpha \rangle \sim -1.73$).

(A color version of this figure is available in the online journal.)

and LBG criteria to $\mathcal{R} = 25.5$ select the majority of galaxies on the bright end of the UV LF, namely those with $L_{UV} \gtrsim 0.1L^*$. We show in the Appendices that these criteria recover the majority of star-forming galaxies fainter than $0.1L^*$. The tests discussed in the Appendices assume that the vast majority of galaxies on the faint end of the UV LF are relatively unreddened, young galaxies. The aim of this section is to quantify the fraction of galaxies on the faint end that are (1) UV-faint simply because they are heavily reddened or (2) older galaxies that have passed their major phase of star formation. The latter investigation is relevant if we are to make inferences on the connection between the dark matter halo mass distribution and the LF.

of what we consider to be "bright" SMGs, and extending the limit to fainter submillimeter fluxes will undoubtedly include galaxies that are less attenuated, on average, and more likely to be recovered via their UV colors (e.g., Reddy et al. 2005; Adelberger & Steidel 2000). In any case, the current best estimates for SMGs that are observed routinely in the first generation of submillimeter surveys imply that by number they make a very small contribution to the number density of sub-L^* galaxies.

Reddy et al. (2006b) demonstrate that the vast majority of luminous infrared galaxies (LIRGs) at $z \gtrsim 2$ will have rest-frame UV colors that satisfy the BX/LBG criteria. While such criteria also pick up a nonnegligible number of ultraluminous infrared galaxies (ULIRGs), the best method of accounting for these galaxies is via their infrared emission. The launch of *Spitzer* enabled observations that are sensitive to the warmer dust in high redshift starburst galaxies. Such galaxies are luminous in the infrared and appear to account for an increasing fraction of galaxies at $z \gtrsim 1$ (e.g., Dey et al. 2008; Caputi et al. 2007; Le Floc'h et al. 2005). Based on such studies, there have been a few estimates of the number density of ULIRGs at $z \sim 2$–3. For instance, Caputi et al. (2007) find a density of $(1.5 \pm 0.2) \times 10^{-4}$ Mpc^{-3} for 24 μm selected galaxies with $L_{\rm bol} \gtrsim 10^{12} L_\odot$ (excluding AGN) in the GOODS fields. Similarly, 24 μm bright galaxies ($f_{24\,\mu{\rm m}} \geqslant 0.3$ mJy) with red optical to mid-IR colors ($R - [24] \geqslant 14$) have a space density in the redshift range $0.5 \leqslant z \leqslant 3.5$ of $(2.82 \pm 0.05) \times 10^{-5}$ Mpc^{-3} (Dey et al. 2008), almost all of which lie below L^*, the characteristic unobscured UV luminosity. Assuming conservatively that all of the ULIRGs of Caputi et al. (2007) are fainter than $\mathcal{R} = 25.5$ and as faint as $\mathcal{R} \sim 28.0$, we find a ULIRG fraction on the UV-faint end of 0.46%. In terms of the Dey et al. (2008) objects, assuming their space density does not evolve between $0.5 \leqslant z \leqslant 3.5$, this fraction is 0.086%. Hence, while such dusty, star-forming galaxies contribute significantly to the total IR luminosity density, they must be vastly outnumbered by galaxies with fainter bolometric luminosities. This result is not surprising given the close-to-exponential drop-off in number counts of such infrared luminous galaxies according to the Schechter function, combined with the steep faint-end slope of the UV LF.

Taken another way, if we make the supposition that a large fraction of galaxies on the faint end of the UV LF are indeed very dusty star-forming ULIRGs, then by virtue of the sheer numbers of UV-faint galaxies, we would predict a number density of ULIRGs significantly in excess of the measured value. These calculations indicate that rapidly star-forming, dusty galaxies constitute a very small fraction of the total number density of star-forming galaxies on the faint end of UV LF. Moreover, they support our premise that the $E(B - V)$ distribution is unlikely to be redder for UV-faint galaxies than for UV-bright ones (Appendices).

7.2. Galaxies with Large Stellar Masses

Another population of galaxies at $z \gtrsim 2$ characterized by their faint UV luminosities are those that have undergone their major episode(s) of star formation and are evolving quiescently (Franx et al. 2003), commonly referred to as "Distant Red Galaxies" or DRGs. Such galaxies have low specific SFRs (Papovich et al. 2006; Reddy et al. 2006b) and are inferred to have low gas fractions (Reddy et al. 2006b) relative to UV-selected galaxies. The bulk of BX/LBGs have stellar masses in the range 10^9–10^{11} $M_\odot$ (Erb et al. 2006; Reddy et al. 2006a; Shapley

et al. 2005), while $K < 20$ DRGs have typical stellar masses of $\gtrsim 10^{11} M_\odot$ (e.g., van Dokkum et al. 2004, 2006), although there is some small overlap in the stellar mass distribution between BX/LBGs and DRGs (Shapley et al. 2005; van Dokkum et al. 2006), particularly at fainter K-band magnitude (Reddy et al. 2005).

van Dokkum et al. (2006) find that galaxies with stellar masses $> 10^{11} M_\odot$ are also typically faint in the optical, with $> 2/3$ fainter than $\mathcal{R} = 25.5$. Conservatively assuming that all such galaxies are fainter than $\mathcal{R} = 25.5$ and as faint as $\mathcal{R} \sim 28.0$, and have an estimated space density of $(2.2 \pm 0.6) \times 10^{-4}$ Mpc^{-3} (van Dokkum et al. 2006), then we compute a fractional contribution to the faint end of the UV LF in the same magnitude range of 0.67%. van Dokkum et al. (2006) noted that only 1/3 of these massive galaxies had the colors of BX/LBGs. However, the examination of their $U_nG\mathcal{R}$ color distribution shows that a large fraction of the "missing" 2/3 have colors that hug the BX/LBG selection boundaries. Our incompleteness corrections will take into account objects that scatter into the BX/LBG samples because of stochastic effects like photometric errors, but conservatively assuming that 2/3 of massive galaxies are missed even after these corrections would imply a massive galaxy fraction among UV-faint sources of $\approx 2\%$.

These estimates imply that like dusty star-forming galaxies, those with large stellar masses ($> 10^{11} M_\odot$) comprise a very small fraction ($\lesssim 2\%$) of all UV-faint galaxies. Hence, virtually all sub-L^* galaxies have smaller stellar masses and are less dusty than the types of galaxies considered above. From a broader perspective, several studies have shown that galaxies with large stellar masses tend to cluster more strongly than less massive galaxies (Quadri et al. 2007; Adelberger et al. 2005a). This is consistent with the expectation that galaxies with large stellar masses formed stars earlier in more massive potential wells which are expected to be the most clustered. Furthermore, Adelberger et al. (2005c) demonstrated that UV-bright galaxies cluster more strongly than UV-faint ones, at least at $z \gtrsim 2$. Given the sheer number of UV-faint galaxies, these observations suggest that galaxies on the faint end of the UV LF are likely to be less clustered than their brighter counterparts, and hence associated with lower mass halos.

8. DISCUSSION: CONSTRAINTS ON THE SFRD

As is customary, the Kennicutt (1998) relation is used to convert UV luminosity to SFR, adopting a Kroupa IMF from 0.1 to 100 $M_\odot$ (Figure 8, Tables 4, 5). This results in a factor of ~ 1.7 decrease in SFR for a given luminosity owing to the larger fractional contribution of high-mass stars to the Kroupa relative to the Salpeter (1955) IMF. For consistency with previous investigations, the luminosity density is calculated to a limiting luminosity of $0.04L^*_{z=3}$ unless stated otherwise. The differential and cumulative unobscured UV luminosity densities to $0.04L^*_{z=3}$, $\rho_{\rm UV}(> 0.04L^*_{z=3})$, are $\approx 6\%$ and 42% larger at $z \sim 2$ and 3, respectively, than reported by R08. This difference is attributable to the steeper faint-end slope and slightly brighter L^* derived in this study. Below, we consider the effects of a luminosity-dependent dust correction, the bolometric LFs at $z \sim 2$–3, and implications for the star-formation history.

8.1. Luminosity-Dependent Dust Corrections

As a consequence of the steep faint-end slopes at $z \sim 2$–3, $\approx 93\%$ of the unobscured UV luminosity density (integrated to zero luminosity) is contributed by galaxies fainter than
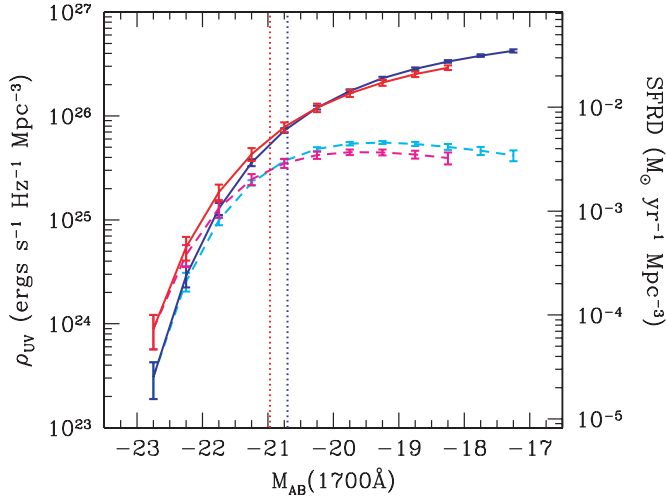
Figure 8. Unobscured UV luminosity density, ρ_{UV}, per 0.5 magnitude interval (dashed lines) and integrated (solid lines) at $1.9 \leqslant z < 2.7$ (cyan, blue) and $2.7 \leqslant z < 3.4$ (magenta, red), respectively. Dotted lines indicate M^* at $z \sim 2$ and $z \sim 3$. The equivalent SFRD assuming the Kennicutt (1998) relation and a Kroupa IMF is shown in the right-hand axis.

(A color version of this figure is available in the online journal.)

Table 4
Total UV Luminosity Densities at $1.9 \leqslant z < 3.4$

Redshift Range	Unobscured[a] (erg s^{-1} Hz^{-1} Mpc^{-3})	Dust Corrected[b] (erg s^{-1} Hz^{-1} Mpc^{-3})
$1.9 \leqslant z < 2.7$	$(3.89 \pm 0.24) \times 10^{26}$	$(1.36 \pm 0.30) \times 10^{27}$
$2.7 \leqslant z < 3.4$	$(3.28 \pm 0.24) \times 10^{26}$	$(8.74 \pm 2.55) \times 10^{26}$

Notes.
[a] Uncorrected for extinction, integrated to $0.04\, L^*_{z=3}$.
[b] Corrected for luminosity-dependent extinction, including both obscured and unobscured UV luminosity, integrated to $0.04\, L^*_{z=3}$.

L^* (Figure 8). The abundance of UV-faint galaxies and their cumulative luminosity makes them ideal candidates for the sources responsible for most of the ionizing flux at $z \gtrsim 3$. However, the luminosity dependence of reddening implies that their contribution to the *bolometric* luminosity is likely to be diminished compared to their contribution to the unobscured

luminosity density. The bolometric luminosity density can be expressed simply as

$$\rho_{UV}^{bol} = \int_L L\phi(L)10^{[0.4k'(\lambda)A(L)]}dL, \qquad (3)$$

where $A(L)$ is the reddening, parameterized by $E(B-V)$, as a function of luminosity and $k'(\lambda)$ is the starburst attenuation relation defined in Calzetti et al. (2000). For this calculation, we have assumed that the bolometric luminosity can be recovered from the rest-frame UV colors—as motivated by *Spitzer* mid-IR observations of UV-selected galaxies (Reddy et al. 2006b)—via the Calzetti et al. (2000) relation. This has been shown to be valid for moderately luminous galaxies (i.e., LIRGs; Reddy et al. 2005, 2006b). We will consider shortly the contribution from high redshift galaxies that do not follow the local starburst attenuation relations (Meurer et al. 1999; Calzetti et al. 2000).

Defining $N(E(B-V), L) \equiv N(E(B-V))$ will of course leave the relative contribution of UV-faint galaxies to ρ_{UV}^{bol} unchanged from their contribution to the unobscured UV luminosity density. The bolometric luminosity density is calculated under the more realistic case of a declining average reddening with unobscured luminosity (Appendices), with the results tabulated in Tables 4 and 5. In this case, we find that galaxies fainter than L^*—defined as the characteristic *unobscured* UV luminosity—contribute 0.62 and 0.78 at $z \sim 2$ and 3, respectively, to ρ_{UV}^{bol} integrated to $0.04L^*_{z=3}$. These fractions are likely to be lower limits since there is a nonnegligible number of very dusty and bolometrically luminous UV-faint galaxies at these redshifts (Section 7). Below, we revisit our estimate of the bolometric luminosity density after incorporating the effect of the most luminous galaxies at $z \sim 2$–3.

8.2. Bolometric Luminosity Functions

Although so far we have defined L^* in terms of the knee of the UV LF uncorrected for extinction, we can also examine the fractional contributions as a function of luminosity to the bolometric luminosity density. This is accomplished by reconstructing the UV LF corrected for extinction using a method similar to that presented in R08. Briefly, a large number of galaxies are simulated with magnitudes and $E(B-V)$ drawn randomly from the LF and luminosity-dependent $E(B-V)$ distribution. The Calzetti et al. (2000) relation is used to recover

Table 5
SFRD Estimates and Dust Correction Factors

	$z \sim 2$		$z \sim 3$	
	$L_{lim} = 0.04L^{*a}$	$L_{lim} = 0$	$L_{lim} = 0.04L^{*a}$	$L_{lim} = 0$
(1) UV SFRD$_{uncor}$[b]	0.032 ± 0.002	0.064 ± 0.003	0.027 ± 0.002	0.055 ± 0.003
(2) UV SFRD$_{cor}$ (LDR)[bc]	0.112 ± 0.025	0.122 ± 0.027	0.072 ± 0.021	0.080 ± 0.023
(3) UV Dust Correction (LDR)[c]	3.50 ± 0.78	1.91 ± 0.42	2.67 ± 0.78	1.45 ± 0.42
(4) UV SFRD$_{cor}$ (CR)[bd]	0.144 ± 0.009	0.288 ± 0.014	0.122 ± 0.009	0.248 ± 0.014
(5) UV Dust Correction (CR)[d]	4.5	4.5	4.5	4.5
(6) Total SFRD$_{cor}$[be]	0.142 ± 0.036	0.152 ± 0.038	0.102 ± 0.032	0.110 ± 0.034
(7) Total Dust Correction[f]	4.44 ± 1.13	2.38 ± 0.59	3.78 ± 1.19	2.00 ± 0.62

Notes.
[a] Integrated to include all galaxies with unobscured UV luminosities brighter than $0.04L^*_{z=3}$, or $M(1700 \text{ Å}) \approx -17.48$.
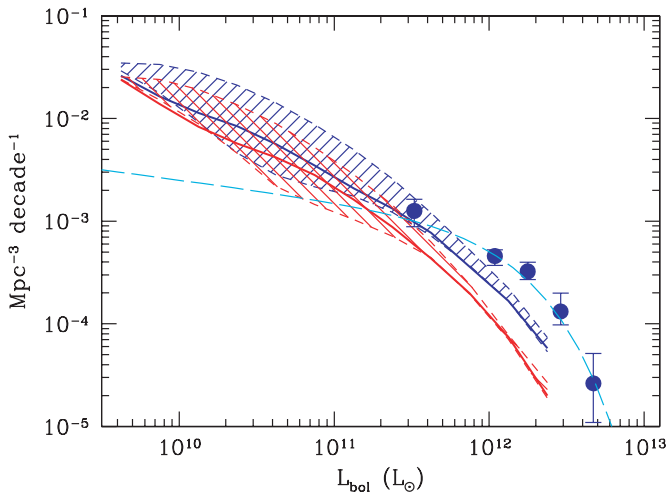[b] In $M_\odot$ yr^{-1} assuming a Kroupa IMF.
[c] Invokes luminosity-dependent reddening (LDR).
[d] Invokes luminosity-invariant reddening (CR).
[e] Sum of LDR-corrected SFRD from row (2) and the contribution of $L_{bol} > 10^{12}$ $L_\odot$ galaxies from Caputi et al. (2007).
[f] Dust correction required to recover total SFRD in row (6) from the unobscured SFRD in row (1).

Figure 9. Bolometric LFs at $z \sim 2$ (blue) and $z \sim 3$ (red), computed by combining the measurement of the UV LF with a luminosity-dependent $E(B-V)$ distribution (see text). The upper limits of the shaded regions indicate the LF derived assuming a constant $E(B-V)$ distribution. The lower limits indicate the LF derived assuming that all galaxies with apparent magnitude fainter than $\mathcal{R} = 25.5$ have zero reddening. These limits encompass the range of likely LFs and give an indication as to the systematic uncertainty in the bolometric LF. The solid lines denote the bolometric LF obtained using our model of the luminosity-dependent $E(B-V)$ distribution that gradually falls to zero reddening for the faintest galaxies. At $z \sim 2$, the higher luminosity points (circles) from Caputi et al. (2007) are shown, along with their Schechter extrapolation to fainter luminosities (long-dashed line).

(A color version of this figure is available in the online journal.)

the bolometric luminosities, which are then binned to produce an LF (Figure 9). We allow for the LF to vary within the errors and add a 0.3 dex scatter to the dust correction implied by $E(B-V)$, reflecting the approximate scatter in both the local relations (Meurer et al. 1999; Calzetti et al. 2000) and those found at $z \sim 2$ (Reddy et al. 2006b). This scatter results in a 5% random error in the faint end of the bolometric LF, significantly smaller than the systematic errors that result from assuming different relations between dustiness and UV luminosity (Figure 9).

Note that we use only the $E(B-V)$ distribution found for UV-selected galaxies to reconstruct the bolometric LFs. The range in attenuation factors obtained for such galaxies will be smaller than the intrinsic range of reddening among all galaxies at $z \sim 2$–3. One obvious reason for this bias is the incompleteness for objects that never scatter into our sample because of their red colors. Another reason is that even if such red, dusty galaxies do satisfy the LBG color criteria, their bolometric luminosities may be underestimated severely based on the UV colors alone. Hence, the method for recovering bolometric LFs based on the $E(B-V)$ distribution of galaxies that scatter into the BX/LBG windows will underestimate the contribution of galaxies to the bright end of the bolometric LF. Because of this, the contribution of these dusty galaxies is based on results published elsewhere. Specifically, we adopt the value of the bright end of the infrared LF at $z \sim 2$ (after exclusion of bright AGNs) presented by Caputi et al. (2007) since the bright end of the bolometric LF should track the bright end of the IR LF. The results are summarized in Figure 9 assuming no evolution in the bright end of the LF ($L_{\rm bol} \gtrsim 10^{12}\,L_\odot$) in the redshift range $1.9 \leqslant z < 3.4$. It is important to keep in mind that νL_ν at 1700 Å scales with SFR in a different way than the infrared luminosity ($L_{\rm IR} \equiv L(8$–$1000\mu)$). Hence, the bolometric luminosity—the

sum of the UV and IR luminosities as defined in this paper—will scale in a nonlinear way with SFR. In the present context, SFRDs are computed separately for (1) galaxies where $L_{\rm bol}$ is determined from the UV-corrected values and (2) galaxies with $L_{\rm bol} \gtrsim 10^{12}\,L_\odot$ where the bolometric luminosity is determined purely from the infrared luminosity (Caputi et al. 2007). The SFRDs from the two contributions are then added to estimate the total. With the appropriate scalings, this calculation implies that ≈ 70–80% of the bolometric luminosity density arises from galaxies with $L_{\rm bol} \lesssim 10^{12}\,L_\odot$, consistent with findings of R08.

Taken together, these findings can be summarized as follows. Including ULIRGs—those galaxies whose UV slopes tend to underpredict their bolometric luminosities (e.g., Papovich et al. 2006, 2007; Reddy et al. 2006b)—does not change the fact that a large portion of the bolometric luminosity density arises from faint galaxies, either those that are fainter than the characteristic unobscured UV luminosity or those that are fainter than the characteristic bolometric luminosity. Placing these results in a wider context will require more precise estimates of the bright end of the bolometric LF that (1) take into account the luminosity-dependent conversion between mid-IR luminosity (upon which most estimates are based) and the total infrared luminosity and (2) the potential contamination from AGN that is prevalent among galaxies with such high IR luminosities. Nonetheless, combining the most recent estimate of the bright end of the bolometric LF (Caputi et al. 2007) with our results at the faint end points to a luminosity density that is dominated by bolometrically faint to moderately luminous galaxies. The implications for a luminosity-dependent reddening distribution on the average dust correction factors applied to high redshift samples and the evolution of the SFRD are discussed in the following sections.

8.3. Average Dust Correction Factors

A luminosity-dependent dust correction and the large ratio of UV-faint to UV-bright galaxies implies an average UV dust correction that is sensitive to the limit of integration used to compute the luminosity density. It seems prudent to consider such a systematic effect given that estimates of the SFRD imply stellar mass densities in excess of what are actually measured (Wilkins et al. 2008). This effect is mentioned in R08; here, we proceed to quantify the average dust correction factors relevant for luminosity densities computed to different limits based on our new determination of the faint-end slope.

The calculated dust corrections and SFRDs are listed in Table 5. We have assumed a contribution of $L_{\rm bol} > 10^{12}\,L_\odot$ galaxies to the SFRD at $z \sim 2$ as computed from Caputi et al. (2007). We also assume this same contribution at $z \sim 3$, though it has not been measured directly at these higher redshifts, in order to place conservative estimates on the effect of a luminosity-dependent dust correction on the average dust correction factors required to convert UV luminosity densities to SFRDs.

The luminosity-dependent reddening model implies dust corrections of a factor of 3.5 and 2.7 at $z \sim 2$ and 3, respectively, integrated to $0.04L^*$ (Table 5), which are up to a factor of two smaller than the typical 4.5–5.0 dust corrections found for $\mathcal{R} \leqslant 25.5$ galaxies (Steidel et al. 1999; Reddy & Steidel 2004). Aside from differences in the luminosity range probed, this difference in average extinction is mitigated somewhat by the fact that a significant fraction (~ 0.2–0.3) of the bolometric luminosity density arises from ULIRGs, where the usual dust conversions do not apply (see discussion above). The expectation is that

the lower dust-corrected luminosity densities inferred in the luminosity-dependent reddening case are compensated by the inclusion of galaxies where $E(B-V)$ tends to underpredict the reddening. The total dust corrections required to recover the bolometric luminosity density, including that contributed by ULIRGs, are 4.4 and 3.8, somewhat larger than the values quoted above. While the differences between these dust corrections may seem small at $z \sim 2$–3, they do result in up to a factor of two in systematic scatter in SFRD measurements, comparable to the dispersion in the local calibrations between luminosity and SFR, and so should be taken into account. The dependency of the average dust correction on the integration limit will be even greater for steeper faint-end slopes given the larger fractional contribution of less reddened faint galaxies to the luminosity density. The average dust correction factors stated above are relevant when integrating the UV LF to $0.04L_{z=3}^*$. Integrating to zero luminosity alters the corrections to be a factor of 2.4 and 2.0 at $z \sim 2$ and 3, respectively. To reiterate, these extinction corrections account for not only the dust obscuration among moderately luminous galaxies prone to UV selection, but also for those ultraluminous galaxies that may either escape UV selection or simply have rest-UV slopes that underpredict their bolometric luminosities. These effects underscore the various subtleties that can affect extinction corrections for UV-selected samples.

Of course, these dust corrections are equally important at higher redshifts $z \gtrsim 3$ where the only constraints on the SFRD come from UV observations. Evidence suggests that UV-selected galaxies become bluer at redshifts $z \gtrsim 3$, relative to galaxies at lower redshifts (Yan & Windhorst 2004; Bouwens et al. 2007).[5] This trend may be attributable to two effects. First, as noted above, L^* evolves strongly as a function of redshift at $z \gtrsim 3$, such that the average UV luminosity of galaxies decreases with increasing redshift. If sub-L^* galaxies have lower dust reddening than UV-bright ones, the trend in UV color may be interpreted as a decrease in dust reddening. A consequence of the luminosity-dependent reddening model is that, when examined over a large dynamic range of luminosity, the unobscured UV luminosity must track the bolometric luminosity, or SFR. This leads to the second effect which is tied to the observation that high redshift galaxies are less attenuated than lower redshift galaxies of the same bolometric luminosity, resulting in a trend of decreasing extinction per unit SFR proceeding to higher redshifts (Reddy et al. 2006b; R08). Stated another way, extrapolating the results of Reddy et al. (2006b) to redshifts $z \gtrsim 4$ implies that higher redshift galaxies are less opaque at UV wavelengths than lower redshift galaxies of the same bolometric luminosity. Hence, the combined effect of a lower L^* and lower average dust attenuation to a given bolometric luminosity implies lower dust corrections at higher z (R08; Bouwens et al. 2007). The implications for this evolution in the average dust correction are discussed in the next section.

There have been several explanations put forth to explain the discrepancy between the integrated star-formation history and stellar mass density measurements, including missing stellar mass, an evolution of the IMF (Davé 2008; van Dokkum 2008), or more generally an evolving conversion between luminosity

and SFR. In light of these effects, we consider the potential impact of an evolving dust correction on the star-formation history, as described below.

9. DISCUSSION: STAR-FORMATION HISTORY AND BUILDUP OF STELLAR MASS

We have already touched upon a few of the implications of a steep faint-end slope on the SFRD. In particular, we noted that a very large fraction of the unobscured UV luminosity density ($\gtrsim 90\%$) arises from galaxies fainter than the characteristic unobscured UV luminosity. Similarly, our results suggest that even assuming a lower reddening among UV-faint galaxies relative to UV-bright ones implies a bolometric, or dust-corrected, luminosity density dominated by galaxies fainter than the characteristic bolometric luminosity. There are several important consequences of these results that we discuss in the next few sections.

### 9.1. Contributions at $z \sim 2$–3 to the Global Stellar Mass Density

A significant fraction of the stellar mass density that formed between $z = 1.9$ and $z = 3.4$ (the redshift limits of our analysis)—corresponding roughly to the epoch when galaxies were forming most of their stars (Section 1)—occurs in galaxies with $L_{\rm bol} \lesssim 10^{12} \, L_\odot$. Using a linear interpolation of the contributions of galaxies with different luminosities to the bolometric luminosity density between $z \sim 3$ and $z \sim 2$ and multiplying by the time between $z = 3.4$ and $z = 1.9$, yields a total SMD of $\Omega_*(1.9 \leqslant z < 3.4) = 0.0014 \pm 0.0003$ in units of the critical density. This value is already 0.57 times that of the present-day value reported in Cole et al. (2001). As mentioned above, there is still a fair amount of uncertainty regarding the bright end of the bolometric LF. Irrespective of the number density of bolometrically luminous galaxies, our calculations suggest that $43 \pm 9\%$ of the present-day stellar mass density was formed in galaxies with $6 \times 10^8 < L_{\rm bol} < 10^{12} \, L_\odot$ between redshifts $z = 3.4$ and 1.9.[6] While much attention recently has been focused on the stellar mass buildup associated with luminous galaxies at high redshift, it is clear that fainter galaxies that are routinely picked up in UV surveys but may be missing from rest-optical and far-IR ones also play an important role. It suggests that much of the stellar mass assembly at a time when galaxies where forming most of their stars occurred in the typical and more numerous galaxies that populate these redshifts.

9.2. Evolution of the SFRD

A luminosity-dependent dust correction not only has consequences for the total SFRD measured at a given redshift, but the strong evolution of L^* suggests that it will induce a systematic effect with redshift. Figure 10 summarizes the SFRDs inferred with the luminosity-dependent reddening model from this study and those of Bouwens et al. (2007) at $z \gtrsim 3.8$, compared with the star-formation history assuming a constant dust correction of 4.5 (red line), along with lower redshift determinations compiled in Hopkins (2004). For consistency with the latter study, we have integrated to zero luminosity (see Section 9.4 for a discussion of the systematic effects associated with the limits

---

[5] It is generally accepted that the highest redshift star-forming populations exhibit bluer UV colors *on average* than similarly selected galaxies at lower redshifts, although the result has not been verified independently with longer wavelength observations. Bouwens et al. (2007) present a discussion of why there may not be a strong bias against dusty galaxies with the higher redshift dropout criteria.

[6] The limit of $6 \times 10^8 \, L_\odot$ is adopted for consistency with R08. The bolometric LF exhibits a slope that is somewhat shallower than the UV LF, so changing the limit of integration to zero bolometric luminosity will add roughly 10% to the luminosity density.
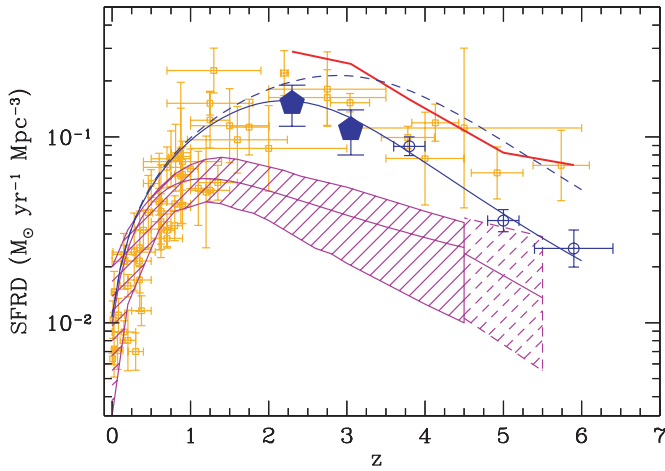
Figure 10. Cosmic star-formation history, including the luminosity-dependent dust-corrected determinations at $z \sim 2$–3 from this analysis (large pentagons) and those of Bouwens et al. (2007) at $z \gtrsim 3.8$ (open circles at high z), and the compilation from Hopkins (2004) (open squares) at low z. Note that our estimates include the directly measured contribution to the SFRD from ULIRGs and assume that this contribution is nonevolving between $z \sim 3$ and $z \sim 2$. Also, for consistency with the Hopkins (2004) compilation, our points and those of Bouwens et al. (2007) are computed by integrating the UV LF to zero luminosity. The solid red line shows the star-formation history assuming a constant dust correction of 4.5 to the unobscured UV luminosity densities at $z \sim 2$–6. The short-dashed line shows the fit to the star-formation history including this constant dust correction model. The solid blue line indicates the best-fit star-formation history assuming a luminosity-dependent dust correction to the $z \gtrsim 2$ measurements. The solid hatched purple region indicates the ± 1 σ star-formation history inferred from the evolution of the stellar mass density (Wilkins et al. 2008), with an extrapolation at $z \gtrsim 4.5$ based on stellar mass density measurements at $z \sim 5$–6 from McLure et al. (2008); Eyles et al. (2007); Stark et al. (2007); Verma et al. (2007); Yan et al. (2006) (dashed purple region). As discussed in the text, much of the discrepancy between the stellar mass density measurements and the integral of the star-formation history may be due to incompleteness of low-mass objects in the stellar mass estimates. A Kroupa IMF is assumed throughout.

(A color version of this figure is available in the online journal.)

of integration). The luminosity-dependent reddening-corrected star-formation history points to a factor of 8–9 increase in the SFRD between $z \sim 6$ and $z \sim 2$ (e.g., see also R08; Bouwens et al. 2007), significantly steeper than the factor of 4 that we would have inferred in the case of a luminosity-invariant (constant) dust correction. As discussed in Section 6.1, the evolution in the unobscured SFRD is connected to the increase in number, and hence luminosity, density of galaxies brighter than L^*. Figure 10 demonstrates that the comparable evolution in the bolometric SFRD is driven both by an increase in the number density of bright galaxies and an evolving dust correction.

The elevated SFRDs predicted in the luminosity-invariant reddening model result in a stellar mass growth of $\Omega_* = 0.0026 \pm 0.0007$ between $2.3 \leqslant z \leqslant 5.9$, compared to $\Omega_* = 0.0013 \pm 0.0003$ for the luminosity-dependent reddening model over the same redshifts, a factor of two difference between the two dust correction scenarios. More importantly, a constant dust correction model predicts stellar mass buildup between $2.3 \leqslant z \leqslant 5.9$ that exceeds the local measurement. Notwithstanding the noted disagreement between stellar mass density measurements and the integral of the star-formation history (Figure 10 and discussion below), these results suggest that we may be able to rule out the elevated SFRs predicted by constant dust correction models, although we caution that the differences in total stellar mass accumulated by $z \sim 2.3$ based on a constant versus declining star-formation history are small

compared to the uncertainties in the SFR and stellar mass density measurements. In the next section, we discuss this disparity between the integrated star-formation history and stellar mass density measurements and possible resolutions.

9.3. Reconciling the Star-Formation History with Stellar Mass Density Measurements: Luminosity-Dependent Dust Corrections and Missing Stellar Mass

Figure 10 shows the star-formation history inferred by differentiating measurements of the stellar mass density (integrated to zero) as a function of redshift (purple hashed region). The results imply that there is a maximum disparity of ≈ 0.5 dex in this inference and actual observations of the SFRD at $z \sim 2$–3. It is of general interest to determine whether this discord is due to some lack of understanding of the fundamental physical processes that govern star formation and/or to the mundane nature of the uncertainties that seemingly plague SFR and stellar mass estimates, including sample incompleteness and the limits to which one integrates to obtain the SFR and stellar mass densities.

In light of the steep faint-end slopes of the UV LF advocated at $z \gtrsim 2$, it is worthwhile to consider the possibility that the stellar mass density measurements at these redshifts are too low, primarily because they do not account for low-mass galaxies that may escape stellar mass selected samples but, even with their low stellar masses, are sufficiently numerous to add appreciably to the total budget of stellar mass. The comparison drawn in Figure 10 implicitly assumes that all the galaxies contributing to the estimate of the SFRD are in some way also represented in the estimate of the stellar mass density. In practice, the problem is that unlike SFR-limited samples, mass-selected samples at high redshift do not probe far enough down the stellar mass function due to the significant amount of time required to assemble the requisite near-IR data. Hence, such studies may underestimate the low-mass slope of the stellar mass function.

9.3.1. Stellar Mass Density in UV-Bright ($\mathcal{R} \leqslant 25.5$) Galaxies

The slope of the stellar mass function at $z \sim 2$–3 is not well constrained. However, if we are able to estimate the average stellar mass of LBGs, then knowing their number density from the UV LF will enable us to estimate their contribution to the stellar mass density. We compiled stellar mass estimates for BXs and LBGs in the GOODS-N and Q1700 fields (Reddy et al. 2006a; Shapley et al. 2005). Briefly, stellar masses are computed for spectroscopically confirmed BXs and LBGs by fitting Bruzual & Charlot (2003) model templates to the observed $U_n G \mathcal{R} + J K_s +$ IRAC photometry, and allowing the star-formation history τ and $E(B - V)$ to vary freely. The SFR and stellar mass are determined by the normalization of the model SED to the broadband photometry (Shapley et al. 2005; Erb et al. 2006; Reddy et al. 2006a).

Excluding spectroscopically identified AGNs, the distributions of stellar mass for 208 BXs and 42 LBGs from the two aforementioned fields are shown in Figure 11. Since most moderately star-forming galaxies escape BX/LBG selection due to stochastic effects (e.g., photometric scatter; Section 3), we adopt the reasonable premise that galaxies to $\mathcal{R} = 25.5$ that do not satisfy the BX/LBG criteria have a similar distribution in stellar masses to those that do. Note that, as discussed previously, this may not be the case for the most massive galaxies at these redshifts (e.g., van Dokkum et al. 2006). However, in the present context we are interested primarily in
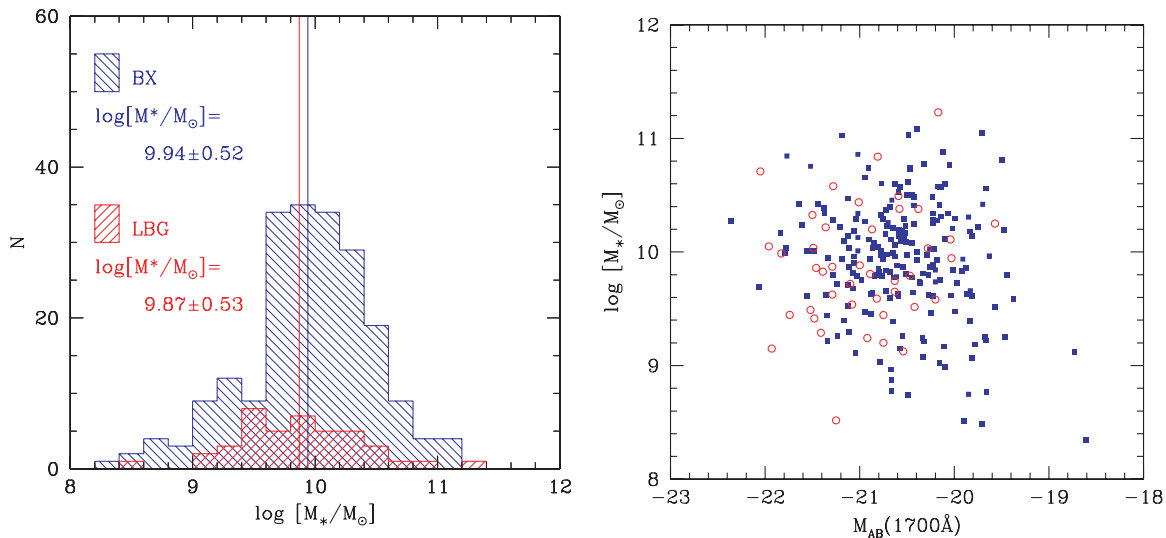
Figure 11. Left: distribution of stellar mass for spectroscopically confirmed BX/LBG galaxies, excluding AGNs, with mean values indicated in the panel and by the vertical lines. Right: stellar mass as a function of unobscured absolute UV magnitude for BX galaxies (filled squares) and LBGs (open circles).
(A color version of this figure is available in the online journal.)

the contribution of *typical* star-forming galaxies—which outnumber by far the most massive galaxies at these redshifts (Section 7)—to the stellar mass density. Furthermore, we show in the Appendices that adopting a young stellar population does not affect appreciably the incompleteness corrections to the BX/LBG samples. Consequently, it is unlikely that large numbers of young galaxies with low stellar masses are scattered out the sample relative to the frequency with which more massive galaxies are scattered out of the sample, particularly among UV-bright galaxies. Therefore, we make the reasonable assumption that the stellar mass distributions for UV-bright BX/LBGs are representative of UV-bright star-forming galaxies in general. Figure 11 also shows the distribution in absolute UV magnitude for galaxies with stellar mass estimates, spanning the full range of magnitudes represented in the spectroscopic sample. As first shown by Shapley et al. (2005), we find no significant correlation between unobscured UV magnitude and stellar mass, perhaps not surprising since the two quantities are related only peripherally. We will revisit this issue below.

Based on these distributions, let us proceed to estimate the stellar mass density contributed by UV-bright galaxies. To do this, we generated many random realizations of the UV LF as allowed by the errors, and drew random absolute magnitudes from each of these realizations. We assigned a stellar mass drawn randomly from the observed distribution (Figure 11), which is then perturbed by 0.3 dex to account for *random* uncertainties (Shapley et al. 2005). The masses are then binned to produce a rough proxy for the stellar mass function. The resulting Gaussian distributions for $\mathcal{R} \leqslant 25.5$ galaxies at $z \sim 2$ and 3—corresponding to galaxies with $M_{AB}(1700\ \text{Å}) \leqslant -19.53$ and -20.05 and $z = 2.3$ and $z = 3.05$, respectively—are shown in Figure 12. Integrating these distributions for those galaxies with $M_* < 10^{11}\ M_\odot$ yields

$$\Omega_*(M_{AB}(1700\ \text{Å}) \leqslant -19.53; < 10^{11}\ M_\odot; z \sim 2.3) \quad (4)$$
$$= (3.72 \pm 0.28) \times 10^{-4}$$
$$\Omega_*(M_{AB}(1700\ \text{Å}) \leqslant -20.05; < 10^{11}\ M_\odot; z \sim 3.05)$$
$$= (1.53 \pm 0.15) \times 10^{-4} \quad (5)$$

in units of the critical density (Table 6). These estimates are meant to reflect the stellar mass densities contributed by

UV-bright star-forming galaxies. Note that the stellar mass densities computed here differ from those derived in Section 9.1; the latter are based on integrating the SFRD, whereas the former are based on masses determined from broadband fitting of galaxy SEDs, and so are subject to somewhat different systematics. The important result of this section is that even without corrections for (1) the most massive and dusty galaxies at these redshifts for which the BX/LBG criteria are incomplete (Section 7) and (2) UV-faint galaxies with $\mathcal{R} > 25.5$, we already find a stellar mass density at $z \sim 2$ comparable to estimates from rest-frame optically selected samples (Figure 12; Fontana et al. 2003; Dickinson et al. 2003; Rudnick et al. 2003; Drory et al. 2005). Of course, direct comparisons between our measurements and those from optically selected samples are fraught with significant biases, both random (e.g., field-to-field variations in the optical samples) and systematic (adopted rest-frame optical limits, underestimates of stellar mass by assuming a single component SF model, or more generally systematics in the assumed M/L ratio and differences in stellar population models). Some of the random uncertainties are constrained by taking values from different surveys conducted in spatially disjoint fields, and at face value, the results above suggest that typical star-forming galaxies already contain an amount of stellar mass comparable to that detected in rest-frame optically selected surveys.

9.3.2. Massive Galaxies

From the survey results of van Dokkum et al. (2004), after converting to a common IMF, the mass density contributed by galaxies with stellar masses $> 10^{11}\ M_\odot$ at $2.0 < z < 3.0$ is $\Omega_*(> 10^{11}\ M_\odot) = (1.64 \pm 0.45) \times 10^{-4}$ (Table 6), where the uncertainty does not include potentially large systematic errors in photometric redshifts (e.g., R08; Shapley et al. 2005). For this calculation, we have assumed that the mass density does not evolve over redshifts $2.0 < z < 3.0$, although it most likely does, and have assumed the aforementioned value is valid at $z \sim 2.3$. Adding this to the contribution from UV-bright galaxies yields a mass density of $\Omega_*(z \sim 2.3) = (5.36 \pm 0.53) \times 10^{-4}$. Do UV-faint galaxies contain enough stellar mass to add appreciably to this number? We explore this question in the next section.
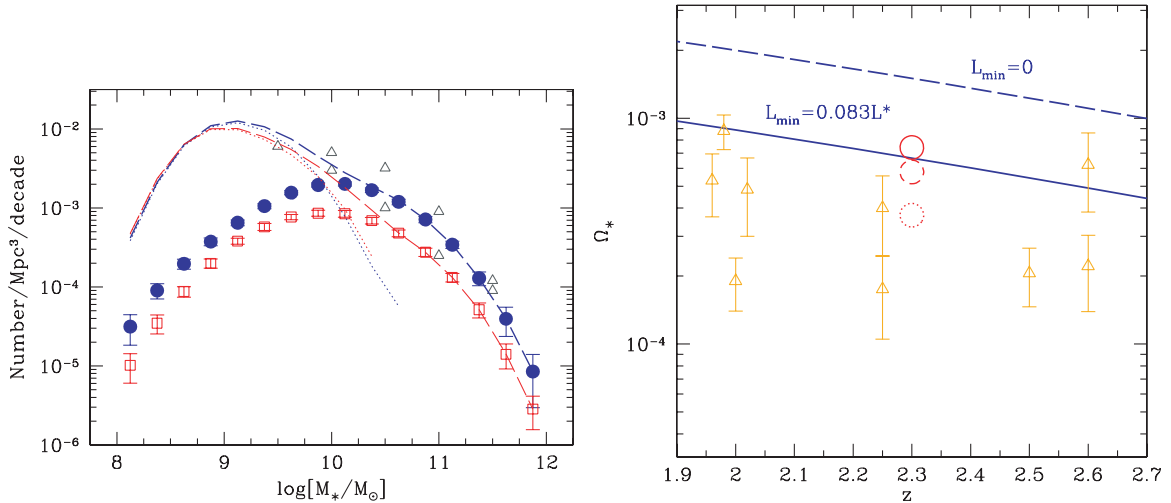
Figure 12. Left: stellar mass functions for $\mathcal{R} \leqslant 25.5$ star-forming galaxies at $1.9 \leqslant z < 2.7$ (filled circles) and $2.7 \leqslant z < 3.4$ (open squares), based on combining the number density computed from the UV LF and the stellar mass distribution measured for BXs and LBGs (Figure 11). The dotted lines indicate the inferred contribution from galaxies fainter than $\mathcal{R} = 25.5$, based on the trend between SFR and stellar mass for UV-selected galaxies (see text). The dashed lines indicate the total contribution from both UV-bright and faint galaxies. For comparison, the GOODS and FDF results at $2.25 < z < 3.00$ from Drory et al. (2005) are denoted by the open triangles. Right: stellar mass density measurements at $1.9 < z < 2.7$ (open triangles) from the following sources: Rudnick et al. (2003); Drory et al. (2005); Pozzetti et al. (2007); Fontana et al. (2003); Dickinson et al. (2003); Fontana et al. (2006). All of these studies constrain the SMD over areas that are significantly smaller than the almost 1 square degree probed in this study, and most rely on photometric redshifts. Our estimates at $z \sim 2.3$ are shown by the large circles: dotted shows the estimate for UV-bright ($\mathcal{R} \leqslant 25.5$) galaxies with $M_* < 10^{11} M_\odot$; dashed shows the estimate including UV-faint galaxies with $M_* < 10^{11} M_\odot$ to a faint limit of $M_{\mathrm{AB}}(1700 \text{ Å}) = -18.0$; and solid denotes the total contribution including massive ($M_* > 10^{11} M_\odot$) galaxies. The stellar mass density inferred by integrating the star-formation history (Figure 10) to a limit of $0.083L^*$ (same as that used to compute the stellar mass density) is denoted by the solid line. For comparison, the dashed line shows the result when integrating the star-formation history to zero luminosity.

(A color version of this figure is available in the online journal.)

9.3.3. Stellar Mass in UV-faint Galaxies

How might the stellar mass distribution be expected to change for UV-faint sub-L^* galaxies? Shapley et al. (2005) and Reddy et al. (2006b) highlight the biases inherent in photometric redshift estimates for star-forming galaxies at $z \sim 2$, perhaps even more so for UV-faint galaxies. We are at present targeting UV-faint galaxies with deep spectroscopy to remedy this situation. Such spectroscopy, combined with deep multiwavelength data in several of our survey fields, should allow us to constrain the stellar populations and masses of sub-L^* to as much confidence as one can obtain with such an analysis. A full SED analysis of such galaxies is beyond the scope of this paper, yet we can make some progress in determining the stellar mass content of sub-L^* galaxies based on observations of UV-bright galaxies.

To do this, we exploited the log–linear relation between SFR and stellar mass found at $z \sim 2.3$ from an analysis of deep HDF data by Sawicki et al. (2007): $\log(M_{\mathrm{stars}}/M_\odot) = 9.0 + 0.86 \log[SFR/(M_\odot \text{ yr}^{-1})]$. They present evidence that this correlation remains valid for galaxies with SFRs of $\approx 1 M_\odot \text{ yr}^{-1}$, corresponding to unobscured UV magnitudes of $M_{\mathrm{AB}}(1700 \text{ Å}) \sim -18.0$. Several other correlations between SFR and stellar mass have been published, including most recently by Reddy et al. (2006b) and Daddi et al. (2007). Adopting these latter relations results in a slightly larger contribution of stellar mass from UV-faint galaxies. Therefore, as a conservative estimate, we have adopted the Sawicki et al. (2007) correlation in the subsequent discussion.[7] Although we do not observe a significant correlation between unobscured UV luminosity and stellar mass for UV-bright ($\mathcal{R} \leqslant 25.5$) galaxies, the log–linear

behavior of SFR with stellar mass implies that such a correlation must exist when examined over a large dynamic range in unobscured UV luminosity. In particular, since UV-faint galaxies are likely to have lower reddening than their brighter counterparts (Section 7), the UV luminosity for these galaxies is expected to track the bolometric luminosity given the tight relation between SFR and reddening (e.g., Reddy et al. 2006a). This, combined with the trend between SFR and M_*, implies a correlation between UV luminosity and stellar mass when examined over a large range in luminosity. Using the procedure outlined above, we recomputed the stellar mass density by integrating the UV LF to $M_{\mathrm{AB}}(1700 \text{ Å}) = -18.00$ and allowing the stellar mass to adjust according to the empirical relation between SFR and M_*. The SFR is determined by combining the absolute magnitude of galaxies with the luminosity-dependent reddening model. The resulting stellar mass densities (Table 6) suggest that roughly as much stellar mass is contained in UV-faint galaxies as is contained in UV-bright ones, implying a relatively steep low-mass slope of the stellar mass function, a conclusion that appears to be a generic result of most cosmological simulations (Nagamine et al. 2004; Finlator et al. 2007). Note that this computation includes only those galaxies that are brighter than $M_{\mathrm{AB}}(1700 \text{ Å}) = -18.00$, since it is down to this limit that the correlation between SFR and M_* has been verified empirically. Assuming the correlation is valid at fainter magnitudes results in a 64% larger stellar mass density contribution from UV-faint galaxies when integrated to $M_{\mathrm{AB}}(1700 \text{ Å}) = -16.00$. For the subsequent discussion, however, we assume the numbers that result from integrating to the brighter limit. More importantly, this discussion highlights the considerable leeway in adjusting the stellar mass density estimates upwards even with conservative assumptions of the stellar mass distribution for UV-faint galaxies.

---

[7] The zero point of the SFR–stellar mass relation appears to evolve with redshift (Noeske et al. 2007). For our analysis, we have assumed the correlation found at $z \sim 2.3$.

Table 6
Stellar Mass Density Budget at $1.9 \leqslant z < 3.4$

	$1.9 \leqslant z < 2.7$	$2.7 \leqslant z < 3.4$
$\Omega_*(\mathcal{R} \leqslant 25.5; < 10^{11}\,M_\odot)$[a]	3.72 ± 0.28	1.53 ± 0.15
$\Omega_*(\mathcal{R} > 25.5; < 10^{11}\,M_\odot)$[b]	2.06 ± 0.26	1.86 ± 0.21
$\Omega_*(> 10^{11}\,M_\odot)$[c]	1.64 ± 0.45	. . .
$\Omega_*(\text{Total})$[d]	7.42 ± 0.59	$> 3.39 \pm 0.26$

Notes.
[a] Stellar mass density, in units of the critical density $\times 10^{-4}$, in galaxies with $\mathcal{R} \leqslant 25.5$ and stellar masses $< 10^{11}\,M_\odot$ assuming a Kroupa IMF.
[b] Same as [a], but includes the contribution inferred for $\mathcal{R} > 25.5$ galaxies based on the correlation between SFR and stellar mass for UV-selected galaxies (see text).
[c] Stellar mass density in galaxies with stellar masses $> 10^{11}\,M_\odot$, based on the data of van Dokkum et al. (2006).
[d] Total stellar mass density, computed by adding the numbers from the first three rows, including the contribution of UV-bright and faint galaxies, as well as those with stellar masses $> 10^{11}\,M_\odot$.

9.3.4. Comparisons with the Integrated Star-Formation History

Can our revised estimate of the stellar mass density at $z \sim 2.3$ account for the star formation that has occurred until then? Figure 12 shows a compilation of stellar mass density estimates from the literature, along with our determinations and the stellar mass density inferred by integrating the luminosity-dependent reddening-corrected star-formation history. Recall that our calculation of the stellar mass density includes galaxies brighter than $M_{\mathrm{AB}}(1700\,\text{Å}) = -18.0$ at $z = 2.3$, corresponding to a luminosity of $0.083L^*$, where L^* is the unobscured characteristic luminosity at $z = 2.3$. When integrating the star-formation history, we must keep track of how these galaxies evolved with time. We have already shown that L^* evolves strongly with redshift, such that $> 0.083L^*_{z=2.3}$ galaxies at $z = 2.3$ would have been fainter on average at higher z. To account for this fading with increasing redshift, we adopt a lower limit to the integral of the UV LF that evolves in the same way as L^*. Specifically, to find the SFRD, we integrate the UV LF to a limit of $0.083L^*$ where, in the integral, L^* varies with redshift. By doing this, we are in effect keeping track of these galaxies' location on the UV LF as a function of time. Note that there may be individual galaxies that contribute to the stellar mass density prior to $z = 2.3$, but then fall below a luminosity of $0.083L^*$ at some later epoch. However, galaxies will of course accumulate most of their stellar mass when they are forming stars at higher rather than lower rate. Furthermore, virtually all of the evolution of the UV LF at $z > 2.3$ can be accommodated by a brightening of L^* with increasing cosmic time (Section 6.1) and, therefore, it is unlikely that there are large numbers of galaxies fading beyond a fixed fraction of L^*. We noted in Section 6 that there is little evolution in the UV LF between $z \sim 4$ and $z \sim 2.3$, but presumably most of the galaxies that are fading are destined to become massive galaxies by $z \sim 2.3$, and recall that our estimate of the stellar mass density at $z \sim 2.3$ *includes* that from massive galaxies with $M_* > 10^{11}\,M_\odot$. Given these reasons, it is reasonable to assume that integrating to $0.083L^*(z)$ should approximate the stellar mass accumulated by galaxies brighter than this limit at all previous epochs.

With this premise, we show the integrated star-formation history in Figure 12. Accounting for the stellar mass content of both UV-bright and faint galaxies results in a stellar mass density at $z = 2.3$ that agrees well with our inference from integrating

the star-formation history. In fact, it is perhaps remarkable that with a simple calculation where we account for the fading of galaxies with increasing cosmic time, we are able to resolve the integrated star-formation history with the global stellar mass density at the very epoch where their supposed disparity reaches its greatest amplitude (Figure 10). A careful analysis of the stellar mass density contributed by galaxies over the bulk of the LF, combined with an integration of the luminosity-dependent reddening-corrected star-formation history to an appropriate limit, may obviate the need to invoke some other mechanism, such as an evolving IMF, to explain the discrepancy. Of course, with the present analysis we cannot rule out that there may be *some* redshift evolution of the IMF, and there are theoretical arguments as to why this may be the case (Larson 1998, 2005). Indeed, such an evolution may plausibly explain the shift in zero point of the trend between SFR and stellar mass as a function of redshift (Davé 2008). All we have shown here is that there is a simpler explanation for the discrepancy between the integrated star-formation history and stellar mass measurements at $z \sim 2$, namely that the former must take into account an evolving dust correction and the latter are likely to be incomplete for galaxies with low stellar masses. In point of fact, incompleteness of stellar mass density measurements and an evolving dust correction are physically well motivated by observations of high redshift galaxies, as we have shown here and elsewhere (Reddy et al. 2006b; R08), whereas IMF evolution has yet to be verified observationally. The results of the last few sections highlight the subtleties that without proper accounting may lead to the types of discrepancies reported in the past. Our findings favor a more nuanced view of the purported discrepancy between the integral of the star-formation history and stellar mass density measurements.

Note that we have not measured directly the stellar mass function at $z \sim 2$, but have inferred it by combining our knowledge of the UV LF (which gives the number density of galaxies) with stellar masses determined from broadband SED fitting. Our analysis suggests that an appreciable fraction of stellar mass is hosted by sub-L^* galaxies and that the steepness of the slope of the stellar mass function may have been underestimated in previous studies based on near-IR data. The robustness of our conclusions should be verified by significantly deeper rest-frame near-IR observations that constrain the low-mass end of the stellar mass function. A more direct sampling of the stellar masses of UV-faint galaxies is required.

9.4. Concluding Remarks

We conclude this section with a few cautionary remarks. As stated previously, we have adopted the $z \gtrsim 4$ measurements of the UV LF that are based on a maximum-likelihood analysis that is most analogous to the method we have used, and that are based on data that extend to comparable depths as achieved here, albeit over an area an order of magnitude smaller, in order to make the most consistent comparison between SFRD estimates. Obvious effects that can contribute to both random and systematic error in the star-formation history include cosmic variance and the limit to which the UV LF is measured. Large-scale multifield surveys at $z \gtrsim 4$ analogous to the present survey at $z \sim 2$–3 will provide better constraints on the random errors associated with cosmic variance. Furthermore, it may be of interest to determine if the similarity in the UV LF from the HDF studies versus the universal one measured at $z \sim 2$–3 (Section 5.4) extends to higher redshifts.

Another point of consideration is the expected turnover in the faint-end slope at very faint luminosities. This turnover is likely dictated by the threshold of cold gas surface density in halos required to trigger star formation (Schmidt 1959; Kennicutt 1998). In the context of the present analysis, the magnitude of the systematic effect that results from integrating the LF to zero luminosity will depend on the steepness of the faint-end slope. For a fixed ϕ^*, the difference between integrating the LF to $0.04L^*$ versus zero luminosity is a factor of 1.85 for $\alpha = -1.73$, 1.44 for $\alpha = -1.6$, and 1.19 for $\alpha = -1.4$. However, at present there are no empirical constraints on the turnover of the faint-end slope of the LF. Even locally, where surveys can probe to luminosities significantly fainter than L^*, there is no evidence for a fall-off in number density of dwarf galaxies. The local u-band LF from the SDSS, for instance, appears to abide by a log–linear relationship between number density and magnitude down to $\approx 0.02L^*$ (Baldry et al. 2005) and, in fact, surveys of the local group of star-forming dwarf galaxies suggest an increasing slope to $0.0001L^*$ (Mateo 1998). Of course, there is no reason why the local rest-frame optical LFs should have the same slope as the rest-frame UV LF, particularly if the LF represents a sequence in mass-to-light ratio. Recall that we have adopted a zero luminosity limit for consistency with the SFRD compilation of Wilkins et al. (2008) and Hopkins (2004). Given the steep faint-end slopes found at $z \gtrsim 2$ and the accommodation of a significant fraction of the luminosity density by faint galaxies, we should bear in mind the possible systematic effects of integrating to zero luminosity, both in terms of the unobscured UV luminosity density and the average dust corrections in the case of luminosity-dependent reddening. A further systematic in the star-formation history may be caused by a redshift dependency in the turnover of the faint-end slope of the UV LF. We note, however, that these systematics will not affect our comparison of the integrated star-formation history and stellar mass density measurements at $z \sim 2$ given that we restricted our analysis to luminosities ($> 0.083L^*$) where we do have empirical constraints on the LF.

It is also worthwhile to mention that the Kennicutt (1998) relation for converting UV luminosity to SFR is valid only for a stellar population age that is $\gtrsim 100$ Myr, since it is after this time that the mix of O and B stars stabilizes assuming a constant star-formation history. For galaxies much younger than this, the UV luminosity will underpredict the SFR based on this relation. Hence, discerning trends in the stellar population age as a function of unobscured UV luminosity is a necessary step in computing accurately the SFRD, particularly since the UV luminosity density appears to be dominated by UV-faint galaxies, if such UV-faint galaxies are systematically younger than their brighter counterparts.

Finally, we note that because the stellar mass density is an integrated quantity, we cannot add arbitrarily large amounts of stellar mass at high redshift without violating the local constraints, assuming the latter are complete in stellar mass. Given that the local measurements can be systematically uncertain by up to 30% (Bell 2003), and the additional contribution from faint galaxies to $M_{AB}(1700 \text{ Å}) = -18.0$ at $z \gtrsim 2$ is only $\approx 9\%$ of the local value, then our finding of significant stellar mass in UV-faint galaxies at $z > 2$ does not pose a problem in terms of the budget of stellar mass in the local universe. In practice, our preliminary estimates of the number density of galaxies with low stellar masses ($M_* \lesssim 10^{10} M_\odot$) may be used to constrain cosmological models that currently predict low-mass slopes of the stellar mass function at $z \gtrsim 3$ that are comparably steep as

the slope of the halo mass function (Nagamine et al. 2008). Ultimately, this issue may be resolved through detailed clustering analysis of sub-L^* galaxies and inferences as to their local descendants. Alternatively, if LAEs represent a short phase in the lifetimes of UV-faint galaxies but are otherwise unremarkable sub-L^* galaxies, then the clustering of LAEs may provide clues to the descendants of UV-faint galaxies (e.g., Kovač et al. 2007; Gawiser et al. 2007).

10. DISCUSSION: EVOLUTION OF THE FAINT-END SLOPE

So far, the discussion has focused on what the UV LFs can tell us about the SFRD and buildup of stellar mass. The modulation of the LF with respect to the underlying halo mass distribution also yields important information regarding the processes that regulate star formation, such as supernovae-driven or radiative winds, and energy injection from AGN, mechanisms generically referred to as "feedback." For example, the sharp cutoff at the bright end of the UV LF may be partly attributable to AGN feedback suppressing star formation in high mass halos (Croton et al. 2006; Scannapieco et al. 2005; Granato et al. 2004), even after taking into account the saturation of UV light with respect to the total SFRs of galaxies with large SFRs (Adelberger & Steidel 2000; Reddy et al. 2006b). Similarly, the shallowness of the faint-end slope of the LF relative to that of the halo mass function suggests some regulating mechanism associated with star formation itself, such as through reionization (Kravtsov et al. 2004; Gnedin 2000), supernovae winds, or radiatively driven winds (Martin 1999; Springel & Hernquist 2003).

One important conclusion from our analysis is that the faint-end slope of the UV LF is relatively constant and steep between $z \sim 2$ and the highest redshifts where α can be measured well, around $z \sim 6$ (Figure 7). At the same time, L^* evolves strongly between these redshifts (Section 6.1). Because the average galaxy is brightening, the invariance of α over these redshifts is not likely reflective of an equilibrium between fading and brightening galaxies. Rather, whatever sub-L^* galaxies at $z \sim 6$ brighten to become L^* galaxies by $z \sim 2$ are made up in number by halos in which gas has newly condensed to form stars by $z \sim 2$.

The steep $\alpha \sim -1.7$ at $z \gtrsim 2$ stands in contrast with the shallower values of $\alpha \sim -1.1$ measured locally (Wyder et al. 2005; Budavári et al. 2005). The redshift evolution of $\alpha(z)$ is summarized in Figure 7 and suggests that most of the change in α occurs mainly below $z \sim 2$. What may be the cause of this change? It has been suggested recently that the evolution in $\alpha(z)$, such that α is shallower at lower redshifts, may reflect the delayed onset of feedback from Type Ia SN (Khochfar et al. 2007). However, even if such feedback is energetically important, it is unclear whether it would have any perceivable effect on $\alpha(z)$ given that the faint-end population evolves strongly between the redshifts in question. A more likely explanation is that the evolution in $\alpha(z)$ is dictated simply by the availability of low-mass halos with cold gas at redshifts $z \lesssim 2$. Perhaps it is not surprising that the apparent shift from steep to shallow faint-end slopes occurs at an epoch ($z \sim 2$) that is marked by a confluence of other important transitions, including the reversal in the evolution of the cosmic star-formation density.

11. CONCLUSIONS

We have used the spectroscopic redshifts and photometric data in all of the fields of the LBG survey to make the most

robust determination of the UV LFs at $1.9 \leqslant z < 2.7$ and $2.7 \leqslant z < 3.4$. Our sample includes over 2000 spectroscopic redshifts, and ≈ 31000 LBGs spread across 31 spatially independent fields over a total area of 3261 arcmin^2. The depth of these data allow us to select LBGs to $0.07L^*$ and $0.1L^*$ at redshift $z \sim 2$ and 3, respectively. The LFs are constrained using a maximum-likelihood procedure that includes the effects of photometric errors, contaminants, and perturbation of galaxy colors due to Lyα. The principal conclusions of this work are as follows:

1. We have quantified the effects of a luminosity dependent reddening and Lyα equivalent width ($W_{Ly\alpha}$) distribution on the incompleteness corrections to our sample. Allowing for a larger fraction of galaxies with large $W_{Ly\alpha}$ among UV-faint galaxies results in a 3–4% increase in the faint-end number densities relative to those obtained by assuming a luminosity-invariant $W_{Ly\alpha}$ distribution as constrained from our spectroscopic sample. Similarly, adopting a luminosity-dependent reddening distribution where the mean reddening of galaxies decreases to fainter UV magnitudes results in an up to 10% increase in the inferred number density of UV-faint galaxies. While these differences in the number density are not negligible, accounting for these luminosity-dependent systematics does little to alter the Schechter parameters, in particular the faint-end slope (α), and it suggests that the UV color criteria are robust to such systematics and that our derived LF must be reasonably complete for UV-faint galaxies. Adopting reasonable assumptions for the luminosity dependence of $W_{Ly\alpha}$ and reddening, we derive faint-end slopes of $\alpha(z = 2) = -1.73 \pm 0.07$ and $\alpha(z = 3) = -1.73 \pm 0.13$.

2. A comparison indicates that our determination yields sub-L^* number densities that are significantly larger, and faint-end slopes that are somewhat steeper, than those published previously. We believe our results are robust given (a) the large number of spectroscopic redshifts used to constrain the bright end of the UV LF, (b) photometry over a large area spread across many spatially independent fields to mitigate cosmic variance, and (c) a careful analysis of the systematics (Lyα line perturbations and luminosity-dependent reddening) that are important for computing the faint-end slope. Our analysis suggests that LFs based on HDF-N data alone are not biased significantly from the universal value of the LF determined here, at least at redshifts $z \sim 2$–3.

3. There is very little evolution in the UV LF in the redshift range $1.9 \leqslant z < 3.4$. However, examined over a larger baseline in redshift and using the published results at $z \sim 6$, we find a brightening of the characteristic unobscured UV magnitude of ~ 1.2 mag between $z \sim 6$ and $z \sim 2$. The faint-end slope remains relatively constant and steep between these redshifts, with a value of $\alpha \sim -1.7$ to -1.8.

4. To examine the frequency of atypical galaxies on the faint end of the UV LF, we compared the number density of sub-L^* galaxies to those of dusty ULIRGs and galaxies with large stellar masses $> 10^{11} M_\odot$. With conservative assumptions regarding their UV magnitude distributions, we find that galaxies with large stellar masses and bolometrically luminous galaxies comprise $\lesssim 2\%$ of the total space density of galaxies fainter than $\mathcal{R} = 25.5$. This small fraction underscores not only the rarity of these objects, but also the large number of UV-faint galaxies implied by the steep faint-end slope.

5. Integrating the UV LFs at $z \sim 2$–3 to zero implies that 93% of the unobscured luminosity density resides in galaxies fainter than L^*. Adopting our prescription for the luminosity dependence of reddening, we construct bolometric LFs to estimate that $> 70\%$ of the bolometric luminosity density arises from galaxies fainter than the characteristic bolometric luminosity at these redshifts. The luminosity-dependent reddening model combined with a steep α implies that the average dust corrections needed to recover the bolometric luminosity density from the unobscured UV luminosity density will depend sensitively on the limit of integration used to compute the luminosity density. Of course, these corrections will also depend on whether they include only the reddening corrections for galaxies routinely selected by their rest-UV colors or if they also include corrections for galaxies that escape UV selection altogether.

6. Assuming a constant reddening correction of 4.5 to the UV-determined star-formation history results in a factor of two overestimate of SFRs and stellar mass densities accumulated at $z \sim 2$–3 relative to the values obtained by assuming a luminosity-dependent reddening correction to the star-formation history. Integrating the latter indicates that at least 25% of the present-day stellar mass density was formed in sub-ultraluminous galaxies between redshifts $z = 3.4$ and $z = 1.9$.

7. The luminosity-dependent reddening-corrected star-formation history points to a factor of 8–9 increase in the SFRD (integrated to zero luminosity) between $z \sim 6$ and $z \sim 2$, significantly steeper than the factor of 4 that we would have inferred in the case of constant dust reddening. The evolution in the bolometric SFRD is driven equally by an evolution in the unobscured characteristic luminosity and an evolving (luminosity dependent) dust correction.

8. We have examined the offset between the integral of the star-formation history and previously published determinations of the stellar mass densities at $z \sim 2$, the epoch where this discrepancy appears to peak in amplitude and where our data are most sensitive. Given the steep faint-end slopes observed at $z \sim 2$, we have explored whether UV-faint galaxies could plausibly account for the observed differences. By summing the stellar mass from all galaxies brighter than $0.083L^*_{z=2}$, we find a stellar mass density that is in remarkable agreement with the luminosity-dependent reddening-corrected star-formation history, when the latter is integrated to the same $0.083L^*$ limit that accounts for the fading of galaxies with increasing cosmic time. This exercise highlights the importance of UV-faint galaxies in the total budget of stellar mass, and suggests that computing the integral of the star-formation history in a way that reflects how galaxies evolve may obviate the need to invoke other mechanisms (e.g., an evolution of the IMF) to reconcile the integrated star-formation history and the global stellar mass density at $z \sim 2$.

9. Finally, while the faint-end slope at any given redshift is likely to be regulated by feedback, discerning the signatures of delayed feedback (e.g., from type Ia SN) in the redshift evolution of α is not trivial, particularly given the strong evolution of the UV LF at $z \gtrsim 2$. Our results suggest that α is roughly constant at $z \gtrsim 2$, contrasting with the shallower values found locally. This evolution may be dictated simply by the availability of low-mass halos capable of supporting star formation at $z \lesssim 2$.

APPENDIX A

TESTING FOR SYSTEMATIC EFFECTS

As discussed in Section 3, the transitional probability function ξ (Equation (2)) is sensitive to changes in the intrinsic properties of galaxies. Our goal is to determine if the resulting modulation of ξ is significant enough to induce a noticeable difference in the maximum-likelihood LF. Since we are interested primarily in computing the UV luminosity distribution of galaxies at these redshifts, we will concentrate on how the reddening, $N(E[B-V])$, and Lyα equivalent width, $N(W_{\mathrm{Ly}\alpha})$, distributions might change with luminosity. More generally, the distributions may also be a function of redshift, but for this analysis we ignore such redshift evolution since there is little published evidence for it over the redshifts considered here (see below). We conclude by discussing the fraction of stellar objects and galaxies outside the redshift ranges of interest.

The most direct approach for testing systematic changes in $N(E[B - V])$ and $N(W_{\mathrm{Ly}\alpha})$ is to examine the LBG color distribution. However, it is difficult from an analysis of the candidates' colors alone to separate the selection effects imposed by the color criteria from those induced by other systematics, such as real changes in the reddening and/or $W_{\mathrm{Ly}\alpha}$ distributions. A different approach takes advantage of the fact that the transitional probability function ξ encapsulates all of the information regarding the selection biases imposed by the color criteria. Therefore, rather than examining directly the color distribution of BXs and LBGs, we chose to make various assumptions of how the reddening and $W_{\mathrm{Ly}\alpha}$ distributions vary as a function of magnitude. Then, based on these assumptions, we recalculated ξ using Monte Carlo simulations and repeated the maximum-likelihood procedure to find the best-fit LF.

A.1. $W_{\mathrm{Ly}\alpha}$ Distribution

There is an increasing body of work that indicates that Lyα emitters (LAEs), those objects selected by narrowband techniques, exhibit significantly larger rest-frame $W_{\mathrm{Ly}\alpha}$, but are much fainter in the continuum, on average, than traditional color-selected galaxies that are restricted to $\mathcal{R} \lesssim 25.5$. Most of these LAEs will lie on the faint end of the UV LF. Adding Lyα emission to a star-forming galaxy's spectrum will tend to scatter such a galaxy out of the BX selection window
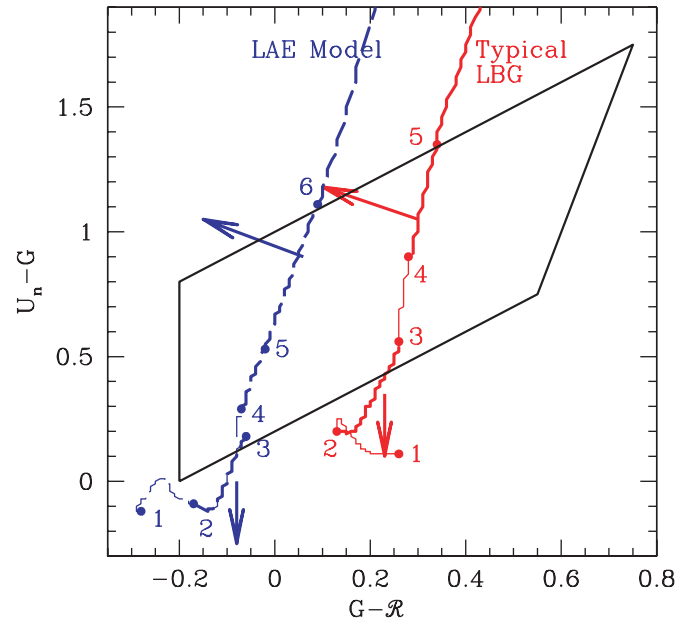
Figure 13. Color tracks for a typical LBG with constant star formation for 100 Myr and $E(B - V) = 0.15$ (solid line) and our model for LAEs with constant star formation for 50 Myr and $E(B - V) = 0$ (no reddening; dashed line). The attenuation of colors due to the IGM has been accounted for following Madau (1995). The labels along each track indicate particular redshifts as follows: (1) $z = 1.00$, (2) $z = 1.68$, (3) $z = 2.17$, (4) $z = 2.48$, (5) $z = 2.65$, and (6) $z = 2.91$. The Lyα line falls in the U_n band at $1.68 \leqslant z < 2.17$ (between points 2 and 3) and in the G band at $z > 2.48$ (above point 4), as indicated by the thicker lines. The effect of *adding* Lyα emission to the spectrum is shown by the arrows, tending to scatter galaxies out of the BX selection window (trapezoid).

(A color version of this figure is available in the online journal.)

(Figure 13).[8] Therefore, for a fixed observed number of faint BX candidates, the incompleteness corrections will be *larger* if they have a distribution skewed toward high $W_{\mathrm{Ly}\alpha}$, thus increasing the inferred number density of faint galaxies. The degree to which the faint-end slope α changes will depend on the $W_{\mathrm{Ly}\alpha}$ distribution, the stellar population distribution, and the number density of high $W_{\mathrm{Ly}\alpha}$ systems. For example, there may be little difference in the faint-end slope derived assuming a high $W_{\mathrm{Ly}\alpha}$ (LAE) population relative to that derived assuming a constant $W_{\mathrm{Ly}\alpha}$ distribution (Section 4) if LAEs constitute a small and constant percentage of galaxies as a function of magnitude on the faint end of the UV LF. We will now consider in detail how a luminosity-dependent $W_{\mathrm{Ly}\alpha}$ distribution affects our analysis.

A.1.1. Assumptions

Here we quantify the effects of a luminosity-dependent $W_{\mathrm{Ly}\alpha}$ distribution by making the following assumptions. First, for ease of discussion, we assume that an "LAE" is any star-forming galaxy with rest-frame $W_{\mathrm{Ly}\alpha} \geqslant 50$ Å, corresponding roughly to the observational lower limits of typical LAE surveys (e.g., Ouchi et al. 2008) and upper $\lesssim 10\%$ of continuum-selected galaxies to $\mathcal{R} = 25.5$ (e.g., Steidel et al. 2003; Shapley et al. 2003; R08). In a strict sense, an LAE is any galaxy with $W_{\mathrm{Ly}\alpha} > 0$, but here we limit ourselves to those that are easily identified using narrowband techniques, to distinguish them from emission line galaxies that are routinely identified from spectroscopy of continuum-selected galaxies. The adoption of

---

[8] For galaxies at $z > 2.48$, where Lyα lies in the G band, the presence of emission will scatter them out of the BX window and into the LBG window (see also Figure 4 of R08).

the $W_{\mathrm{Ly}\alpha} = 50$ Å cutoff is for reference purposes only, and does not affect the subsequent analysis since a separate assumption is made regarding the median value of $W_{\mathrm{Ly}\alpha}$ for LAEs. In particular, the simulations are performed using different values of $W_{\mathrm{Ly}\alpha}$ ranging from 50 Å to 250 Å (rest-frame), the latter being a canonical upper limit for standard assumptions of the IMF (Salpeter 1955) and solar metallicity (Charlot & Fall 1993).

Second, we adopt an average stellar population consistent with the most recent analyses of LAEs at high redshift. The range of ages found for LAEs is ∼ 10 Myr at the low end to ∼ 1 Gyr at the high end, with typical ages of ∼ 100–200 Myr, and low metallicity and reddening (e.g., Gronwall et al. 2007; Ouchi et al. 2008). We conservatively assume an average LAE age of 50 Myr, metallicity of $1/20\, Z_{\odot}$, and zero dust reddening for the purposes of our simulation. For illustrative purposes, Figure 13 shows the colors as a function of redshift for such a stellar population compared to a model that represents the typical LBG with age > 100 Myr and $E(B-V) \sim 0.15$ (assuming the BC06 model). As discussed above, irrespective of whether Lyα lies in the U_n or G band, the effect of adding emission is to scatter galaxies at $1.9 \leqslant z < 2.7$ out of the BX selection window.

Third, we must determine the frequency of LAEs among the general star-forming population as a function of continuum magnitude. Ouchi et al. (2008) determine the UV LF of LAEs with $W_{\mathrm{Ly}\alpha} \gtrsim 50$ Å at $z \approx 3.1$ and find it to be fitted adequately with a Schechter form of the LF with $\phi^* = (5.6^{+6.7}_{-3.1}) \times 10^{-4}$ Mpc^{-3} and $M^*_{1500\,\text{Å}} = -19.8 \pm 0.4$ with a fixed faint-end slope of $\alpha_{\mathrm{LAE}} = -1.6$. Integrating the continuum-UV LF of LAEs and comparing with the UV LF determined above for all star-forming galaxies implies an LAE fraction (ϵ) that is a strong function of magnitude, ranging from less than 0.02% in the brightest magnitude bin ($-22.83 \leqslant M(1700\,\text{Å}) < -22.33$) to $\approx 9.3\%$ in the faintest bin ($-18.33 \leqslant M(1700\,\text{Å}) < -17.83$). Note that the fraction of LAEs on the faint end is based on an extrapolation of the UV LF of LAEs assuming $\alpha = -1.6$ (Ouchi et al. 2008). Furthermore, the fractions will go up (or down) depending on whether we decrease (or increase) the limiting $W_{\mathrm{Ly}\alpha}$ that segregates LAEs from other galaxies (e.g., using a limit of $W_{\mathrm{Ly}\alpha} = 20$ Å instead of 50 Å). In our simulations, we assume (1) no evolution in the UV LF of LAEs between $z \sim 2$–3 and (2) a fraction of LAEs that varies with absolute magnitude in accordance with our findings above, with a fraction of 10% for $W_{\mathrm{Ly}\alpha} > 50$ Å in the faintest bin considered here.

To recap, the main assumptions going forward are that LAEs are described by a 50 Myr stellar population with no reddening and comprise anywhere from $< 0.02\%$ to 10%, respectively, of galaxies within the bright and faint magnitude bins of our analysis. In the next section, we consider how different values of $W_{\mathrm{Ly}\alpha}$ among LAEs affects the faint end of the UV LF of all star-forming galaxies.

A.1.2. Effect of a Changing $W_{\mathrm{Ly}\alpha}$ Distribution

With the aforementioned premises, the UV LF is computed for varying amounts of emission among the LAEs, with equivalent widths from 50 Å to 250 Å. In our simple model, the luminosity-dependent $W_{\mathrm{Ly}\alpha}$ distribution can be expressed as

$$N(W_{\mathrm{Ly}\alpha}, \mathcal{R}) = [1 - \epsilon(\mathcal{R})]N_{\mathrm{o}}(W_{\mathrm{Ly}\alpha}) + \epsilon(\mathcal{R})\delta(\omega), \quad \text{(A1)}$$

where $N_{\mathrm{o}}(W_{\mathrm{Ly}\alpha})$ is the distribution for $\mathcal{R} \leqslant 25.5$ galaxies (Figure 1), $\epsilon(\mathcal{R})$ is the $W_{\mathrm{Ly}\alpha} > 50$ Å fraction as a function
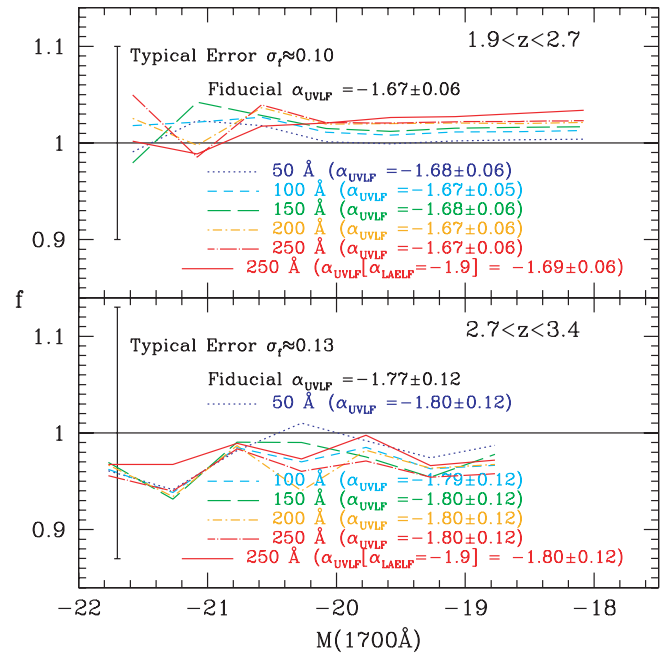
Figure 14. Comparison of maximum-likelihood number density of galaxies as a function of magnitude for (1) our fiducial UV LFs assuming that *all* galaxies abide by the $W_{\mathrm{Ly}\alpha}$ distribution seen for bright ($\mathcal{R} \leqslant 25.5$) continuum-selected galaxies (Figure 1) and (2) the UV LFs derived assuming a population of LAEs with high $W_{\mathrm{Ly}\alpha}$ at faint magnitudes. The different lines show the ratio of the LFs determined from (2) to that determined from (1), and correspond to differing amounts of Lyα emission attributed to the LAE population. The typical error in this ratio (σ_f) is shown by the vertical error bar. In all cases, we find that such a population of high $W_{\mathrm{Ly}\alpha}$ systems does little to alter the faint-end slope of the UV LF.

(A color version of this figure is available in the online journal.)

of magnitude as determined above, and $\delta(\omega)$ is a delta function with center at $\omega = 50, 100, 150, 200,$ and 250 Å.[9] The results at $z \sim 2$ and $z \sim 3$ (Figure 14) are presented in terms of the ratio of the number density (η^*) for different values of $W_{\mathrm{Ly}\alpha}$ for LAEs to the number density (η) derived using the fiducial $W_{\mathrm{Ly}\alpha}$ distribution for $\mathcal{R} \leqslant 25.5$ continuum-selected galaxies (e.g., Figure 1),

$$f = \frac{\eta^*}{\eta}, \quad \text{(A2)}$$

with error given by

$$\sigma_f = \frac{\left[\eta^2 \sigma_{\eta^*}^2 + (\eta^*)^2 \sigma_{\eta}^2\right]^{1/2}}{\eta^2}. \quad \text{(A3)}$$

The error in number density σ_{η^*} is determined in exactly the same manner as the error in the LF (σ_{η}; Section 4). Even with the most conservative assumption for the $W_{\mathrm{Ly}\alpha}$ attributed to LAEs (an assumed value of $W_{\mathrm{Ly}\alpha} = 250$ Å), we find that inclusion of such a population alters the faint-end number densities at a 2–4% level depending on the redshift. Not surprisingly, at lower redshifts, $1.9 \leqslant z < 2.7$, the inclusion of LAEs increases the inferred number densities at the faint end by $\lesssim 3\%$, since such galaxies would be preferentially scattered out of the BX

---

[9] The intrinsic distribution for UV-bright galaxies (Figure 1) also includes a small fraction of continuum-selected galaxies with $W_{\mathrm{Ly}\alpha} \geqslant 50$ Å. We ignore this small overlap between the continuum and LAE $W_{\mathrm{Ly}\alpha}$ distributions, with the obvious consequence of slightly increasing the total fraction of galaxies with $W_{\mathrm{Ly}\alpha} \geqslant 50$ Å.

selection window. The opposite is found at higher redshifts ($2.7 \leqslant z < 3.4$), where the number density is systematically lower by up to 4%, primarily because there are more LAEs scattered from $z < 2.7$ into the LBG selection window than are (at any redshift $2.7 \leqslant z < 3.4$) scattered out of the window, assuming no evolution of the UV LF of LAEs at the redshifts of concern. Hence, for a fixed number of $z \sim 3$ LBG candidates, the tendency would be to overestimate the number density had we not accounted for the LAE population.

The expectation of a steepening α for the universal UV LF (i.e., for all star-forming galaxies) at $z \sim 2$ when including LAEs is not borne out with our simulations for several reasons. First, the overall fraction of LAEs, even at the faint end of the UV LF, is small ($\lesssim 10\%$). Their effect on the LF is further diminished because they will only affect the broadband colors if they are at particular redshifts (Figure 13). Second, the current determination of the UV LF of LAEs assumed a fixed $\alpha_{\mathrm{LAE}} = -1.6$ (Ouchi et al. 2008), which is not too different from the fiducial α (Section 4). Thus, while the fraction of LAEs among the general population is a strong function of magnitude between our brightest and faintest magnitude bin, it is in fact a relatively constant ≈ 8–9% for bins fainter than $M(1700\,\text{Å}) \approx -20$. Adopting a steeper faint-end slope of the UV LF of LAEs of $\alpha_{\mathrm{LAELF}} = -1.9$ still results in a universal faint-end slope (α_{UVLF}) that is consistent with the fiducial value (Figure 14).

Future studies that constrain more robustly α_{LAELF} over the *entire* redshift range probed here will be useful for assessing the overall impact of high $W_{\mathrm{Ly\alpha}}$ systems on the faint-end slope inferred for all star-forming galaxies. It is also not unreasonable to suspect disparate absorption properties between UV bright versus faint galaxies, so *spectroscopic* studies, while difficult to carry out at present, are crucial for assessing the variation of $W_{\mathrm{Ly\alpha}}$ with luminosity (e.g., Shapley et al. 2003).

Nonetheless, while the inclusion of high $W_{\mathrm{Ly\alpha}}$ systems among the UV continuum-faint population may be a small systematic effect (3–4%), it is not negligible compared to the error in number density at the faint end of the UV LF (10–15%), and so should be included in any proper assessment of the UV LF. The critical point, and one that is demonstrated unambiguously with our simulations (Figure 14), is that such a systematic effect does little to alter the faint-end slope of the universal LF.[10] In our final determination of the LF, we have made the conservative assumption of a median value of $W_{\mathrm{Ly\alpha}} = 150\,\text{Å}$ for the LAE population with $W_{\mathrm{Ly\alpha}} > 50\,\text{Å}$ (although, as noted above, the exact value does little to alter the LF). The resulting best-fit Schechter parameters are listed in Table 7.

APPENDIX B

REDDENING DISTRIBUTION

B.1. Test Cases

In the previous section, we assumed a young stellar population and no reddening when modeling LAEs. In this section, we test for modulation in the LF if *all* UV-faint galaxies are characterized with a young stellar population and lower reddening than UV-bright galaxies. In this case, the LAEs would simply represent a phase of UV-faint galaxies with a short duty cycle

---

[10] While the small change in the $W_{\mathrm{Ly\alpha}}$ distribution brought on by the inclusion of LAEs does little to alter the faint-end slope, significant discrepancies in the faint end of the UV LF arise when not accounting at all for the $W_{\mathrm{Ly\alpha}}$ distribution of galaxies at these redshifts (R08).

of $\lesssim 10\%$, based on the number density of LAEs compared to the general continuum population (e.g., Kovač et al. 2007; Nagamine et al. 2008; Verhamme et al. 2008; Gawiser et al. 2007). Note that here we are concerned with the changing distribution of reddening of galaxies as a function UV magnitude *at a given epoch*. A somewhat related issue is how the reddening distribution in general shifts to lower values at higher redshift for galaxies of a given SFR (R08; see also Section 8).

The first case under consideration is if the average $E(B - V)$ of galaxies with $\mathcal{R} > 25.5$ is zero. This scenario would be the most conservative one we can make for two reasons. First, R08 demonstrate using UV continuum-slopes and *Spitzer* MIPS data that the reddening distribution of UV-selected galaxies does not vary significantly to the spectroscopic limit of $\mathcal{R} \sim 25.5$. Because this limit is arbitrary with respect to galaxy properties, we would not expect the reddening to change so suddenly for galaxies fainter than this limit and indeed it would be unphysical. A more meaningful model is one in which the average reddening asymptotes to zero proceeding to fainter luminosities (R08). Second, there is a nonnegligible fraction of galaxies at $z \sim 2$–3 on the faint end of the UV LF that are bolometrically luminous and dusty (e.g., Chapman et al. 2005; van Dokkum et al. 2004). Yet, a large fraction of these galaxies have colors and UV opacity that do not differ significantly from those of UV continuum-bright objects (Chapman et al. 2005; Reddy et al. 2005, 2006b; R08). By assuming an average reddening that falls to zero for galaxies fainter than $\mathcal{R} = 25.5$, we are effectively seeking the *maximal* change in the LF under such a scenario. We also consider a more physical reddening distribution whose mean $\langle E(B - V) \rangle$ decreases monotonically from a value of $\langle E(B - V) \rangle \sim 0.13$ at $\mathcal{R} = 25.5$ to zero at the faintest apparent magnitude bin of our analysis (case 2). With this model, galaxies at the faint end of the UV LF ($M(1700\,\text{Å}) \approx -18.00$) will have close to zero reddening, similar to the mean reddening (as inferred from the rest-UV slopes) of dropout galaxies at $z \sim 6$ with comparable unobscured UV luminosities (Bouwens et al. 2006). If we define the $N(E(B - V))$ distribution for galaxies brighter than $\mathcal{R} = 25.5$ as

$$N[E(B - V), \mathcal{R} \leqslant 25.5] \equiv N_0, \qquad (\text{B1})$$

then our model for the luminosity dependence of $N(E(B - V), \mathcal{R})$ can be written as

$$
\begin{aligned}
N(E(B - V), \mathcal{R}) = N_0, \quad & \mathcal{R} \leqslant 25.5 \\
= f(\langle E(B - V) \rangle, \sigma(N_0)), & \\
& \mathcal{R} > 25.5, \qquad (\text{B2})
\end{aligned}
$$

where the function $f(\langle E(B - V) \rangle, \sigma(N_0))$ is a Gaussian with mean $\langle E(B - V) \rangle = 0$ (Case 1) and $\langle E(B - V) \rangle = -0.09\mathcal{R} + 2.43$ (Case 2) and dispersion equivalent to that observed for N_0 (i.e., $\sigma(N_0)$). Note that while N_0 is not in fact distributed normally, the differences that arise by assuming a Gaussian are negligible. Furthermore, for simplicity we have assumed that the dispersion of the $E(B - V)$ distribution is independent of magnitude. R08 argue for an increased dispersion at faint magnitudes due to the mixing of galaxies with intrinsically low SFRs and those that are UV-faint because of high extinction. The effect of such an increasing dispersion is to reduce the effective volume of the survey and thus the incompleteness corrections will be larger at the faint end. In general, however, because the number density of UV-faint galaxies with little reddening is inferred to be much larger than that of heavily reddened UV-faint galaxies (Section 7), the increase in dispersion attributable

Table 7
Best-Fit Schechter Parameters for UV LFs of $1.9 \lesssim z \lesssim 3.4$ Galaxies

Redshift Range	Systematic Effect	α	$M^*_{AB}(1700\ \text{Å})$	ϕ^* ($\times 10^{-3}$ Mpc^{-3})
$1.9 \leqslant z < 2.7$	Fiducial[a]	-1.67 ± 0.06	-20.65 ± 0.08	2.84 ± 0.42
	$W_{Ly\alpha} = 150\ \text{Å}$[b]	-1.68 ± 0.06	-20.68 ± 0.08	2.83 ± 0.42
	$[E(B-V)]_{grad}$[c]	-1.72 ± 0.06	-20.71 ± 0.09	2.64 ± 0.46
	Combined[d]	-1.73 ± 0.07	-20.70 ± 0.11	2.75 ± 0.54
$2.7 \leqslant z < 3.4$	Fiducial[a]	-1.77 ± 0.12	-20.98 ± 0.13	1.54 ± 0.43
	$W_{Ly\alpha} = 150\ \text{Å}$[b]	-1.80 ± 0.12	-21.06 ± 0.13	1.34 ± 0.42
	$[E(B-V)]_{grad}$[c]	-1.78 ± 0.12	-20.97 ± 0.13	1.55 ± 0.43
	Combined[d]	-1.73 ± 0.13	-20.97 ± 0.14	1.71 ± 0.53

Notes.
[a] Fiducial LF assumes no change in the $W_{Ly\alpha}$ and $E(B-V)$ distributions as a function of UV apparent magnitude.
[b] LF derived assuming an LAE population at the faint end with $W_{Ly\alpha} = 150$ Å (see text).
[c] LF derived assuming a linearly declining mean $E(B-V)$ for galaxies with $\mathcal{R} > 25.5$ (see text).
[d] LF derived combining the effects of a changing $W_{Ly\alpha}$ and $E(B-V)$ distribution as a function of UV apparent magnitude.

to the latter is likely to be negligible. In addition, at the faintest magnitudes where $\langle E(B-V)\rangle$ approaches zero, the dispersion will be dominated not by reddening but by the intrinsic variation in SEDs of galaxies. Consequentially, the dispersion will likely be smaller than the $\sigma(N_0)$ measured at brighter magnitudes. Note that there is a nonnegligible number of galaxies in the spectroscopic sample that have measured $E(B-V) < 0$. Since we use $E(B-V)$ as an indicator of dust, we set a lower limit of $E(B-V) = 0$ for any galaxies that happen to be assigned a negative value. Finally, R08 demonstrate that the mean extinction among galaxies above a particular unobscured luminosity is roughly constant with redshift between $1.9 \leqslant z < 3.4$. Motivated by this, we adopt nonevolution of reddening in the simulations; i.e., $N(E(B-V), \mathcal{R}, z) \approx N(E(B-V), \mathcal{R})$. For brevity in the subsequent discussion, the abbreviation ZR refers to the case of a discontinuous reddening distribution such that galaxies with $\mathcal{R} > 25.5$ have $E(B-V) = 0$. Similarly, LDR refers to our analytical model for the luminosity-dependent reddening distribution that has reddening decreasing monotonically with UV magnitude.

B.2. Results

The results are summarized in Figure 15 for both case 1 (ZR), where all galaxies with $\mathcal{R} > 25.5$ have $E(B-V) = 0$, and case 2 (LDR), where the mean reddening decreases with magnitude. There are several conclusions of import. Focusing on the lower redshift galaxies, in the ZR case we find a significant increase of up to 70% in the inferred number density of galaxies with $M(1700\ \text{Å}) > -20$ relative to that inferred from the fiducial model. This can be understood by examining Figure 13. Galaxies with no reddening (e.g., as in the case of the LAE model) have bluer colors that approach the boundary of the BX color selection window. Thus, photometric errors preferentially scatter galaxies out of the selection window compared to typical BXs. The net effect is that for a fixed number of observed BX candidates, the incompleteness corrections will be larger, leading to larger number densities. We find a statistically insignificant difference between the fiducial and ZR faint-end slopes, attributable to the fact that the reddening distribution is fixed to have $\langle E(B-V)\rangle = 0$. A gradually declining distribution (case 2; LDR), results in number densities that are up to ≈ 10% larger and a slightly steeper faint-end slope, although the parameters of the Schechter function are still consistent with

those of the fiducial case within their respective marginalized errors.

The luminosity-dependent variation of the $E(B-V)$ distribution has less of an effect on the faint-end number densities in the higher redshift range $2.7 \leqslant z < 3.4$, primarily because the LBG criteria include colors that are much bluer than those expected for even a young and unreddened stellar population. However, because we account also for the intrinsic scatter in $N(E(B-V))$, the differences in faint-end number densities are still somewhat larger than we would have obtained had we modeled the $N(E(B-V))$ distribution as a δ function at a given $\mathcal{R}$-band magnitude (i.e., assuming all galaxies at a given $\mathcal{R}$ have the same reddening). In any case, the LBG criteria are somewhat more robust to extreme assumptions regarding the $E(B-V)$ distribution of UV-faint galaxies compared to the BX criteria. Simply altering the BX criteria to include candidates with bluer $G - \mathcal{R}$ colors could alleviate some of this difference, but we note that our deep photometry indicates that galaxies with such blue colors ($G - \mathcal{R} \lesssim -0.2$) are rare. For the purposes of our present analysis, the exact placement of the color criteria is not important as long as the effect of the criteria is modeled appropriately and incompleteness is accounted for using a likelihood analysis.

Deep spectroscopy combined with multiwavelength indicators of the extinction of sub-L^* galaxies is required to more robustly constrain the $E(B-V)$ distribution as a function of unobscured UV luminosity. For the time being, however, we have shown that adopting simple scenarios for how the distribution changes with UV luminosity results in a faint-end slope that can be potentially steeper at $z \sim 2$ than we would have obtained by assuming a constant $E(B-V)$ distribution. For our final determination of the UV LF, we have adopted our prescription for the luminosity dependence of reddening, namely one in which the reddening declines linearly with apparent magnitude, as discussed above. The resulting best-fit Schechter parameters are listed in Table 7.

APPENDIX C

OBJECTS OUTSIDE THE REDSHIFT RANGES OF INTEREST

Intrinsic variations in the SEDs of star-forming galaxies and photometric errors lead to significant wings of the redshift
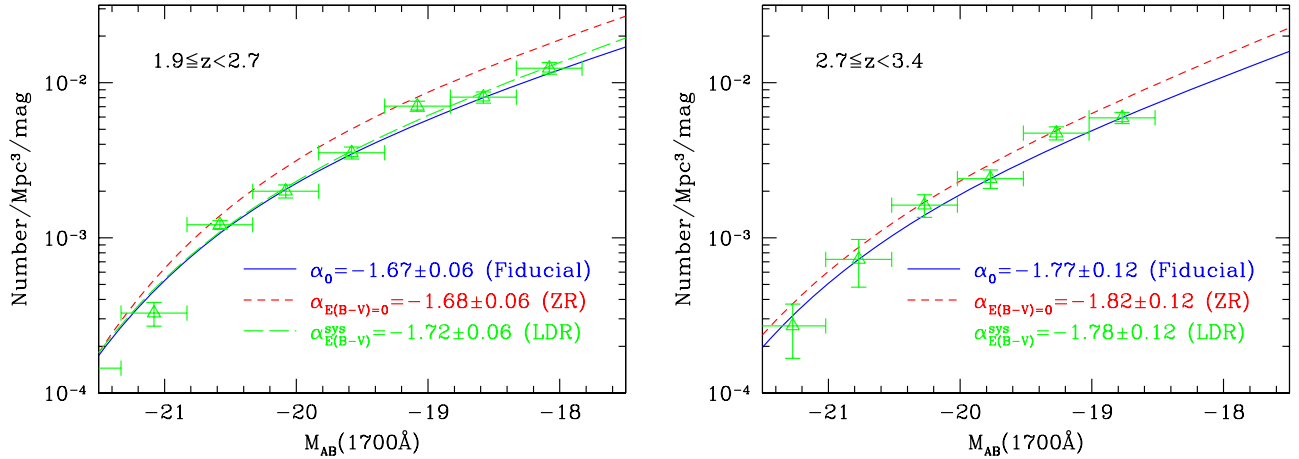
Figure 15. Change in faint-end slope of the UV LF assuming that galaxies with $\mathcal{R} > 25.5$ have (1) $\langle E(B - V) \rangle = 0$ ($\alpha_{E(B-V)=0}$) and (2) $\langle E(B - V) \rangle$ that falls off linearly with magnitude ($\alpha_{E(B-V)}^{\text{sys}}$), compared to the fiducial value that assumes galaxies have the same $\langle E(B - V) \rangle \approx 0.13$ irrespective of apparent magnitude (α_0). For clarity, data points are shown only for case (2) in both panels and the Schechter fit for case (2) is excluded from the right panel.

(A color version of this figure is available in the online journal.)

selection functions, $N(z, L)$, for color-selected samples. Here, the selection function is parameterized in terms of both redshift and luminosity. In this analysis, we have computed the LFs specifically over the redshift ranges $1.9 \leqslant z < 2.7$ and $2.7 \leqslant z < 3.4$, although the exact redshift interval used is unimportant since the LF does not evolve over these redshifts (see R08 and Section 6). More importantly, we estimate the fraction of photometric candidates that fall in the redshift ranges over which the LFs are computed, information that is provided directly from the spectroscopic sample.

In the faintest apparent magnitude bin of the spectroscopic sample, $25.0 \leqslant \mathcal{R} < 25.5$, the observed fractions of galaxies (excluding AGNs/QSOs) that fall in the ranges $1.9 \leqslant z < 2.7$ and $2.7 \leqslant z < 3.4$ are 77% and 72%, respectively (virtually all of the objects that are outside these redshift ranges still have $z > 1$ since the contamination due to $z \leqslant 1$ objects is very small at these faint magnitudes—see R08). In the previous analysis, the fractions of 77% and 72% are assumed to remain constant for galaxies fainter than $\mathcal{R} = 25.5$. There are at least a couple of reasons why this is likely to be a reasonable assumption. First, the contamination from $z < 1$ objects to the photometric sample is a strong function of magnitude. If this trend continues to fainter magnitudes, then we would expect the $z < 1$ contamination rate to be less than 1% for objects fainter than $\mathcal{R} = 25.5$. Adopting zero contamination from $z < 1$ objects at $\mathcal{R} > 25.5$ results in number densities at the faint end that are $\approx 1\%$ larger. This is an insignificant change given the magnitude of the other systematics discussed above. In theory, the larger photometric errors for UV-faint objects may result in an increase of the contamination rate at the faint end. A small sample of 15 spectroscopically confirmed galaxies with $25.5 < \mathcal{R} < 26.0$ in the Q1422 field (Steidel et al. 2003; R08) implies a zero contamination fraction. Larger spectroscopic samples of UV-faint objects will be required to obtain a statistically robust estimate of contamination at the faint end. However, all of the previous studies that have attempted to constrain the faint end of the UV LF (Steidel et al. 1999; Sawicki & Thompson 2006) also assume negligible contamination at the faint end. Hence, the difference between our determination of a steep-faint end slope and the shallower values found elsewhere (see Section 5.1) cannot be attributable to differences in the assumed contamination rate as a function of UV luminosity.

Second, the redshift distribution for UV-selected galaxies will be modulated primarily by systematics that affect the overall colors of galaxies at these redshifts, namely Lyα perturbations and the $E(B - V)$ distribution, such that $N(z, L) = f(N[W_{\text{Ly}\alpha}], N[E(B - V)])$. From this discussion, we conclude that the redshift distribution likely remains similar between UV-bright and faint galaxies (i.e., $N(z, L) \approx N(z)$). It is easy to see, however, the potential danger of assuming that $N(z)$ is insensitive to luminosity: even gradual changes in the stellar population and reddening of galaxies as a function of magnitude may result in an artificial suppression of the faint end of the UV LF with respect to the bright end. This motivates the need for selection criteria that are efficient at targeting galaxies with a wide range of intrinsic properties at the desired redshifts (see the next section).

For the selection criteria adopted here, the presence of high $W_{\text{Ly}\alpha}$ systems and/or a bluer population of UV-faint galaxies does little to alter the parameterization of the maximum-likelihood LF under reasonable assumptions for LAE number densities and the reddening distribution. In other words, the modulation of $N(z, L)$, and more generally ξ, the transitional probability function, due to these systematic effects do not affect appreciably our LF determination. Substantial changes in the redshift distribution *can* arise from a rapid evolution of the LAE number density and $E(B - V)$ distributions over the redshifts of concern. However, lacking evidence that such evolution is occurring—and, as discussed above, there is little evolution in the $E(B - V)$ distribution over these redshifts; R08)—it is likely that the redshift distributions of BXs and LBGs with $\mathcal{R} > 25.5$ is similar to those of $\mathcal{R} < 25.5$ galaxies.

APPENDIX D

IMPLICATIONS FOR COLOR SELECTION AT HIGH REDSHIFT

It is instructive to take a broader view and examine the significance of the tests described here in the context of the color selection criteria. The primary result of this section is that the systematics brought about by reasonable assumptions for the unobscured UV luminosity dependence of the $W_{\text{Ly}\alpha}$ and reddening distributions do little to alter our inference of the UV LF *for the selection criteria used here*. We emphasize the

latter part since obviously some sets of criteria will be more susceptible to modulations of $N(W_{Ly\alpha})$ and $N(E[B - V])$ than others. As has been discussed elsewhere (Steidel et al. 2003, 2004; Adelberger et al. 2004), the goal of observing efficiency dictates that a balance be struck between the inclusion of as many galaxies at the redshifts of interest as possible and the exclusion of as many foreground or background contaminants. In the context of the present analysis, luminosity-dependent properties of galaxies should also be taken into account when designing color criteria. UV-dropout criteria are in general the most efficient method for selecting high redshift galaxies. Because they target preferentially bluer galaxies, the luminosity-dependent systematics expected for UV-faint galaxies works in favor of their selection via rest-frame UV emission. In contrast, near-IR selections that target redder galaxies (either because they are dusty, have large stellar masses, or both), may potentially miss an appreciable fraction of galaxies that populate the faint end of the UV LF (Section 7). Hence, the aggregate of these selection methods provides a complementary view and are necessary for obtaining an unbiased census of star formation.

Obviously, incompleteness corrections for criteria that target blue galaxies are not completely immune to extreme luminosity-dependent gradients in $N(E[B - V], \mathcal{R})$, for example (Figure 15). The power of our simulations and maximum-likelihood method is that they can be used to quantify and correct for even severe biases (e.g., in the faint-end slope) imposed by high redshift galaxy selection in a way that is not possible with the traditional methods of computing LFs (see discussion in R08). The keystone of our entire method is the spectroscopy: while not extending fainter than the typical ground-based magnitude limit, spectroscopy for UV-bright galaxies does provide a critical foundation, or "zero point," for assessing how luminosity-dependent systematics may affect our inferences of the faint end. Using these techniques, we showed in R08 that, after correcting for low redshift objects and AGNs/QSOs based on extensive spectroscopy, the UV LF inferred by magnitude-limited surveys is similar to that derived from color-selected surveys. Hence, we argued that we must be complete for UV-bright galaxies. The slight modifications of the Schechter parameterization of the LF after taking into account $N(W_{Ly\alpha}, \mathcal{R})$ and $N(E[B - V], \mathcal{R})$ implies that our determination must also be reasonably complete for UV-faint galaxies.

REFERENCES

Adelberger, K. L., Erb, D. K., Steidel, C. C., Reddy, N. A., Pettini, M., & Shapley, A. E. 2005a, ApJ, 620, L75
Adelberger, K. L., Shapley, A. E., Steidel, C. C., Pettini, M., Erb, D. K., & Reddy, N. A. 2005b, ApJ, 629, 636
Adelberger, K. L., & Steidel, C. C. 2000, ApJ, 544, 218
Adelberger, K. L., Steidel, C. C., Pettini, M., Shapley, A. E., Reddy, N. A., & Erb, D. K. 2005c, ApJ, 619, 697
Adelberger, K. L., Steidel, C. C., Shapley, A. E., Hunt, M. P., Erb, D. K., Reddy, N. A., & Pettini, M. 2004, ApJ, 607, 226
Adelberger, K. L., Steidel, C. C., Shapley, A. E., & Pettini, M. 2003, ApJ, 584, 45
Alexander, D. M., Bauer, F. E., Chapman, S. C., Smail, I., Blain, A. W., Brandt, W. N., & Ivison, R. J. 2005, ApJ, 632, 736
Arnouts, S., et al. 2005, ApJ, 619, L43
Baldry, I. K., et al. 2005, MNRAS, 358, 441
Barger, A. J., Cowie, L. L., Sanders, D. B., Fulton, E., Taniguchi, Y., Sato, Y., Kawara, K., & Okuda, H. 1998, Nature, 394, 248
Beckwith, S. V. W., et al. 2006, AJ, 132, 1729
Bell, E. F. 2003, ApJ, 586, 794
Bertin, E., & Arnouts, S. 1996, A&AS, 117, 393
Bouwens, R. J., Illingworth, G. D., Blakeslee, J. P., & Franx, M. 2006, ApJ, 653, 53
Bouwens, R. J., Illingworth, G. D., Franx, M., & Ford, H. 2007, ApJ, 670, 928
Bouwens, R. J., Illingworth, G. D., Franx, M., & Ford, H. 2008, ApJ, 686, 230
Bruzual, G., & Charlot, S. 2003, MNRAS, 344, 1000
Budavári, T., et al. 2005, ApJ, 619, L31
Bunker, A. J., Stanway, E. R., Ellis, R. S., & McMahon, R. G. 2004, MNRAS, 355, 374
Calzetti, D., Armus, L., Bohlin, R. C., Kinney, A. L., Koornneef, J., & Storchi-Bergmann, T. 2000, ApJ, 533, 682
Caputi, K. I., et al. 2007, ApJ, 660, 97
Chapman, S. C., Blain, A. W., Smail, I., & Ivison, R. J. 2005, ApJ, 622, 772
Charlot, S., & Fall, S. M. 1993, ApJ, 415, 580
Cole, S., et al. 2001, MNRAS, 326, 255
Conroy, C., Shapley, A. E., Tinker, J. L., Santos, M. R., & Lemson, G. 2008, ApJ, 679, 1192
Coppin, K., et al. 2006, MNRAS, 372, 1621
Croton, D. J., et al. 2006, MNRAS, 365, 11
Daddi, E., et al. 2007, ApJ, 670, 156
Davé, R. 2008, MNRAS, 385, 147
Dekel, A., & Birnboim, Y. 2006, MNRAS, 368, 2
Dey, A., et al. 2008, ApJ, 677, 943
Dickinson, M., et al. 2004, ApJ, 600, L99
Dickinson, M., Papovich, C., Ferguson, H. C., & Budavári, T. 2003, ApJ, 587, 25
Drory, N., Salvato, M., Gabasch, A., Bender, R., Hopp, U., Feulner, G., & Pannella, M. 2005, ApJ, 619, L131
Erb, D. K., Steidel, C. C., Shapley, A. E., Pettini, M., Reddy, N. A., & Adelberger, K. L. 2006, ApJ, 646, 107
Eyles, L. P., Bunker, A. J., Ellis, R. S., Lacy, M., Stanway, E. R., Stark, D. P., & Chiu, K. 2007, MNRAS, 374, 910
Finlator, K., Davé, R., & Oppenheimer, B. D. 2007, MNRAS, 376, 1861
Fontana, A., et al. 2003, ApJ, 594, L9
Fontana, A., et al. 2006, A&A, 459, 745
Franx, M., et al. 2003, ApJ, 587, L79
Gabasch, A., et al. 2004, ApJ, 616, L83
Gawiser, E., et al. 2007, ApJ, 671, 278
Giavalisco, M., et al. 2004a, ApJ, 600, L103
Giavalisco, M., et al. 2004b, ApJ, 600, L93
Gnedin, N. Y. 2000, ApJ, 542, 535
Granato, G. L., De Zotti, G., Silva, L., Bressan, A., & Danese, L. 2004, ApJ, 600, 580
Gronwall, C., et al. 2007, ApJ, 667, 79
Groth, E. J., Kristian, J. A., Lynds, R., O'Neil, E. J., Jr., Balsano, R., Rhodes, J., & WFPC-1 IDT. 1994, BAAS, 26, 1403
Hopkins, A. M. 2004, ApJ, 615, 209
Hughes, D. H., et al. 1998, Nature, 394, 241
Iwata, I., Ohta, K., Tamura, N., Akiyama, M., Aoki, K., Ando, M., Kiuchi, G., & Sawicki, M. 2007, MNRAS, 376, 1557
Iwata, I., Ohta, K., Tamura, N., Ando, M., Wada, S., Watanabe, C., Akiyama, M., & Aoki, K. 2003, PASJ, 55, 415
Kennicutt, R. C. 1998, ARA&A, 36, 189
Khochfar, S., Silk, J., Windhorst, R. A., & Ryan, R. E., Jr. 2007, ApJ, 668, L115
Kovač, K., Somerville, R. S., Rhoads, J. E., Malhotra, S., & Wang, J. 2007, ApJ, 668, 15
Kravtsov, A. V., Berlind, A. A., Wechsler, R. H., Klypin, A. A., Gottlöber, S., Allgood, B., & Primack, J. R. 2004, ApJ, 609, 35
Kroupa, P. 2001, MNRAS, 322, 231
Larson, R. B. 1998, MNRAS, 301, 569
Larson, R. B. 2005, MNRAS, 359, 211
Le Fèvre, O., et al. 2005, Nature, 437, 519
Le Floc'h, E., et al. 2005, ApJ, 632, 169
Lilly, S. J., Le Fevre, O., Hammer, F., & Crampton, D. 1996, ApJ, 460, L1
Lilly, S. J., Tresse, L., Hammer, F., Crampton, D., & Le Fevre, O. 1995, ApJ, 455, 108
Madau, P. 1995, ApJ, 441, 18
Madau, P., Ferguson, H. C., Dickinson, M. E., Giavalisco, M., Steidel, C. C., & Fruchter, A. 1996, MNRAS, 283, 1388
Martin, C. L. 1999, ApJ, 513, 156
Mateo, M. L. 1998, ARA&A, 36, 435
McLure, R. J., Cirasuolo, M., Dunlop, J. S., Foucaud, S., & Almaini, O. 2008, arXiv:0805.1335
Meurer, G. R., Heckman, T. M., & Calzetti, D. 1999, ApJ, 521, 64
Nagamine, K., Ouchi, M., Springel, V., & Hernquist, L. 2008, arXiv:0802.0228
Nagamine, K., Springel, V., Hernquist, L., & Machacek, M. 2004, MNRAS, 350, 385

Noeske, K. G., et al. 2007, ApJ, 660, L43
Ouchi, M., et al. 2004, ApJ, 611, 660
Ouchi, M., et al. 2008, ApJS, 176, 301
Paltani, S., et al. 2007, A&A, 463, 873
Papovich, C., et al. 2006, ApJ, 640, 92
Papovich, C., et al. 2007, ApJ, 668, 45
Poli, F., Menci, N., Giallongo, E., Fontana, A., Cristiani, S., & D'Odorico, S. 2001, ApJ, 551, L45
Pozzetti, L., et al. 2007, A&A, 474, 443
Prochaska, J. X., & Tumlinson, J. 2008, arXiv:0805.4635
Quadri, R., et al. 2007, ApJ, 654, 138
Reddy, N. A., Erb, D. K., Steidel, C. C., Shapley, A. E., Adelberger, K. L., & Pettini, M. 2005, ApJ, 633, 748
Reddy, N. A., & Steidel, C. C. 2004, ApJ, 603, L13
Reddy, N. A., Steidel, C. C., Erb, D. K., Shapley, A. E., & Pettini, M. 2006a, ApJ, 653, 1004
Reddy, N. A., Steidel, C. C., Fadda, D., Yan, L., Pettini, M., Shapley, A. E., Erb, D. K., & Adelberger, K. L. 2006b, ApJ, 644, 792
Reddy, N. A., Steidel, C. C., Pettini, M., Adelberger, K. L., Shapley, A. E., Erb, D. K., & Dickinson, M. 2008, ApJS, 175, 48
Rees, M. J., & Ostriker, J. P. 1977, MNRAS, 179, 541
Rudnick, G., et al. 2003, ApJ, 599, 847
Ryan, R. E., Jr., et al. 2007, ApJ, 668, 839
Salpeter, E. E. 1955, ApJ, 121, 161
Sawicki, M., et al. 2007, in ASP Conf. Ser. 380, Deepest Astronomical Surveys, ed. J. Afonso, H. C. Ferguson, B. Mobasher, & R. Norris (San Francisco, CA: ASP), 433
Sawicki, M., & Thompson, D. 2006, ApJ, 642, 653
Scannapieco, E., Silk, J., & Bouwens, R. 2005, ApJ, 635, L13
Schechter, P. 1976, ApJ, 203, 297
Schmidt, M. 1959, ApJ, 129, 243
Shapley, A. E., Steidel, C. C., Erb, D. K., Reddy, N. A., Adelberger, K. L., Pettini, M., Barmby, P., & Huang, J. 2005, ApJ, 626, 698
Shapley, A. E., Steidel, C. C., Pettini, M., & Adelberger, K. L. 2003, ApJ, 588, 65
Silk, J., & Rees, M. J. 1998, A&A, 331, L1
Smail, I., Ivison, R. J., & Blain, A. W. 1997, ApJ, 490, L5
Spergel, D. N., et al. 2007, ApJS, 170, 377
Springel, V., & Hernquist, L. 2003, MNRAS, 339, 312
Stark, D. P., Bunker, A. J., Ellis, R. S., Eyles, L. P., & Lacy, M. 2007, ApJ, 659, 84
Steidel, C. C., Adelberger, K. L., Giavalisco, M., Dickinson, M., & Pettini, M. 1999, ApJ, 519, 1
Steidel, C. C., Adelberger, K. L., Shapley, A. E., Pettini, M., Dickinson, M., & Giavalisco, M. 2003, ApJ, 592, 728
Steidel, C. C., Shapley, A. E., Pettini, M., Adelberger, K. L., Erb, D. K., Reddy, N. A., & Hunt, M. P. 2004, ApJ, 604, 534
Trenti, M., & Stiavelli, M. 2008, ApJ, 676, 767
Valdes, F. 1982, FOCAS User's Manual (Tucson, AZ: NOAO)
van Dokkum, P. G. 2008, ApJ, 674, 29
van Dokkum, P. G., et al. 2004, ApJ, 611, 703
van Dokkum, P. G., et al. 2006, ApJ, 638, L59
Verhamme, A., Schaerer, D., Atek, H., & Tapken, C. 2008, A&A, 491, 89
Verma, A., Lehnert, M. D., Förster Schreiber, N. M., Bremer, M. N., & Douglas, L. 2007, MNRAS, 377, 1024
Wilkins, S. M., Trentham, N., & Hopkins, A. M. 2008, MNRAS, 385, 687
Wyder, T. K., et al. 2005, ApJ, 619, L15
Yan, H., Dickinson, M., Giavalisco, M., Stern, D., Eisenhardt, P. R. M., & Ferguson, H. C. 2006, ApJ, 651, 24
Yan, H., & Windhorst, R. A. 2004, ApJ, 612, L93
Yan, L., et al. 2007, ApJ, 658, 778
Yoshida, M., et al. 2006, ApJ, 653, 988